Actinomycin D and bortezomib disrupt protein homeostasis in Wilms tumor

Patricia D.B. Tiburcio[1], Kenian Chen[2], Lin Xu[1,2], Kenneth S. Chen[1,3 *]

[1] Department of Pediatrics, University of Texas Southwestern Medical Center, Dallas, TX
[2] Quantitative Biomedical Research Center, Peter O'Donnell School of Public Health, University of Texas Southwestern Medical Center, Dallas, TX
[3] Children's Medical Center Research Institute, University of Texas Southwestern Medical Center, Dallas, TX

* Correspondence: Kenneth S. Chen, UT Southwestern Medical Center, 5323 Harry Hines Blvd., Dallas, TX 75390; phone: +1-214-648-8291; email: Kenneth.Chen@UTSouthwestern.edu

The authors have no conflicts of interest to disclose.

ABSTRACT

Wilms tumor is the most common kidney cancer in children, and diffusely anaplastic Wilms tumor is the most chemoresistant histological subtype. Here we explore how Wilms tumor cells evade the common chemotherapeutic drug actinomycin D, which inhibits ribosomal RNA biogenesis. Using ribosome profiling, protein arrays, and a genome-wide knockout screen, we describe how actinomycin D disrupts protein homeostasis and blocks cell cycle progression. We found that, when ribosomal capacity is limited by actinomycin D treatment, anaplastic Wilms tumor cells preferentially translate proteasome components and upregulate proteasome activity. Furthermore, the proteasome inhibitor bortezomib sensitizes cells to actinomycin D treatment by inducing apoptosis both *in vitro* and *in vivo*. Lastly, we show that increased levels of proteasome components are associated with anaplastic histology and with worse prognosis in non-anaplastic Wilms tumor. In sum, maintaining protein homeostasis is critical for Wilms tumor proliferation, and it can be therapeutically disrupted by blocking protein synthesis or turnover.

36 **INTRODUCTION**

37

38 Wilms tumors, or nephroblastomas, are the most common pediatric kidney cancer.
39 Globally, Wilms tumor is diagnosed in 10.4 per 1 million children less than 15 years old each
40 year [1]. North American risk stratification criteria classify Wilms tumors as having favorable or
41 anaplastic histology. The development of effective combinations of chemotherapy, radiation,
42 and surgery has pushed the 5-year overall survival rate to over 90% for those with favorable
43 histology Wilms tumor (FHWT). These strong cure rates have allowed us to de-intensify therapy
44 for FHWT, where up to 24% of long-term survivors who were treated on historical regimens
45 developed therapy-related chronic health conditions [2]. On the other hand, patients with
46 diffusely anaplastic Wilms tumor (DAWT), which accounts for ~10% of Wilms tumor patients,
47 continue to have a relapse rate of over 40% and a 4-year overall survival rate of 66% despite
48 being treated with more aggressive drugs such as doxorubicin, etoposide, cyclophosphamide,
49 and carboplatin [1,3-5]. Recent attempts to intensify chemotherapy for those with DAWT have
50 increased short-term toxicity with minimal improvements in cure rate [6]. Anaplastic histology is
51 associated with loss or mutation of p53 [7,8], but the molecular mechanisms underpinning
52 chemoresistance in anaplasia are unknown, and there remain no targeted therapies effective in
53 Wilms tumor.

54 Since the 1960s, chemotherapy regimens utilizing actinomycinD (actD), also called
55 dactinomycin, have been routinely used to treat Wilms tumors [9,10], rhabdomyosarcoma, and
56 other sarcomas [11,12]. In DAWT, however, actD has been replaced by doxorubicin, which can
57 provide higher rates of cure but carries significantly more short- and long-term toxicity [13]. It is
58 unknown why DAWT is less sensitive to actD. Understanding how to improve actD sensitivity
59 and avoid the toxicities associated with anthracyclines like doxorubicin could improve outcomes
60 for Wilms tumor as well as other malignancies.

61 ActD is a DNA-intercalating agent that can block transcription and DNA replication at
62 high concentrations. However, at the low-nanomolar serum concentrations typically achieved in
63 patients, it primarily inhibits transcription of ribosomal RNA (rRNA), which is transcribed by RNA
64 polymerase I (Pol I) and transfer RNA (tRNA), which is transcribed by RNA polymerase III (Pol III)

65 [14-18]. Ribosomes are composed of rRNA and ribosomal proteins (RP), and impaired Pol I activity
66 results in fewer fully formed ribosomes, which consequently reduces global translation. In
67 ribosome-depleted settings, the remaining ribosomes are not uniformly distributed across
68 remaining transcripts; instead, they favor certain transcripts, based on factors such as their
69 intracellular localization, secondary structure, and presence of specific sequence motifs [18,19]
70 (Supplementary Figure S1A). We thus reasoned that preferentially translated genes following
71 actD exposure could be targetable vulnerabilities in anaplastic Wilms tumor cells. To date,
72 however, no published findings have characterized how actD affects translation in Wilms
73 tumors.
74 In this study, we used ribosome profiling to find that proteasome components are
75 preferentially translated in anaplastic Wilms tumor cell lines following actD treatment. The
76 proteasome inhibitor bortezomib (BTZ) increases sensitivity of anaplastic Wilms tumor cells to
77 actD *in vitro* and *in vivo*. Lastly, DAWTs express higher levels of proteasome components than
78 FHWTs, and higher levels of proteasome components are associated with worse prognosis.
79

MATERIALS AND METHODS

Tissue culture

The anaplastic, *TP53*-mutated Wilms tumor cell line WiT49 (RRID: CVCL_0583) was maintained in Dulbecco's Modified Eagle Medium (DMEM) with 1000 mg/L glucose, 4 mM L-glutamine, 1 mM pyruvate (Gibco 11995065) supplemented with antibiotic-antimycotic (Gibco 15240062) and fetal bovine serum (Sigma F2442) to 10% final concentration in 37°C at 5% CO_2. A second anaplastic, *TP53*-mutated Wilms tumor cell line 17.94 (Ximbio 153333, RRID:CVCL_D704) was grown in DMEM supplemented with antibiotic-antimycotic and heat inactivated fetal bovine serum (Gibco 16140063) to 20% final concentration in 37°C at 5% CO_2. Cell line identity is annually verified by short tandem repeat genotyping (last verified February 2024 for WiT49 and April 2024 for 17.94). They are also tested biannually for mycoplasma contamination (Latest negative screen February 2024, Lonza LT07-318).

Ribosomal RNA quantification

To determine the effect of actD on rRNA expression, WiT49 or 17.94 cells were seeded at ~50% confluency in 3 different plates. The following day, cells were treated with either vehicle (DMSO) or 2nM actD for 6 hours or 24 hours. At experiment endpoint, total RNA was extracted using the miRNeasy kit with DNase I digestion (Qiagen 217004 and 79254), and cDNA synthesis was performed with iScript™ Reverse Transcription Supermix (Bio-Rad 1708841). Quantitative PCR (qPCR) was performed using iTaq™ Universal SYBR® Green Supermix (Bio-Rad 1725125) with primers listed: *18s* rRNA (GTAACCCGTTGAACCCCATT, CCATCCAATCGGTAGTAGCG); *45s* pre-rRNA (ACCCACCCTCGGTGAGA, CAAGGCACGCCTCTCAGAT); *GAPDH* (CGGAGTCAACGGATTTGGT, ACCAGAGTTAAAAGCAGCCC). Relative expression was calculated by the $2^{-\Delta\Delta Ct}$ method by normalizing each rRNA species to *GAPDH*. Significance was determined by unpaired two-tailed Student's T-test versus vehicle control.

109 **Protein synthesis quantification**

110

111 To determine the effect of actD on protein synthesis, WiT49 cells were seeded at ~30%
112 confluency in cell culture chamber slides. The following day, cells were treated with either
113 vehicle (DMSO) or 2nM actD for 48 hours or 72 hours. At the endpoint, protein synthesis was
114 measured using a fluorescence-based O-propargyl-puromycin (OPP) incorporation kit
115 (Invitrogen C10457) according to manufacturer protocols. Nuclei were counterstained with DAPI
116 (4',6-diamidino-2-phenylindole). Each condition was photographed at 5 non-overlapping regions
117 at 20x magnification on a BZ-X810 Fluorescence microscope (Keyence Corporation) and
118 quantified using Fiji [20]. Necrotic regions were disregarded. Relative fluorescence units were
119 calculated from the blue (DAPI) and red (OPP-Alexa Fluor 488) channels. The number of nuclei
120 was counted from the DAPI channel using the Watershed and Analyze Particles functions in Fiji.
121 Raw protein synthesis was calculated as the average red fluorescence intensity in pixels with any
122 fluorescence using the Area and Integrated Density functions in Fiji. For each image, raw
123 protein synthesis was then normalized to the number of nuclei in that field of view. Each field of
124 view was treated as a replicate, and statistical analysis was performed by unpaired two-tailed
125 Student's t-test against untreated cells.

126

127 **Reverse phase protein array**

128

129 WiT49 cells at 20% density were treated with 1 nM actD or DMSO as vehicle control for
130 72 hours in duplicate. 1×10^6 cells were collected, washed, and frozen in liquid nitrogen, and sent
131 to the MD Anderson Functional Proteomic Reverse Phase Protein Array Core [21-23]. Normalized,
132 log2-transformed, median-centered values from "validated" antibodies were used for analysis
133 [24]. The log2-fold-change for each antibody was calculated as the difference between the means
134 of actD-treated and DMSO-treated samples, and the standard deviation for each antibody was
135 calculated as the standard deviation of all four values.

136

137 **Ribosome profiling**

138

139 WiT49 cells were incubated in complete growth medium with 2nM actD or DMSO for 6
140 or 72 hours, in three replicates per condition. For 2-week long treatments, WiT49 were
141 maintained and passaged in two 7-day cycles of drug/vehicle-supplemented media for 3 days,
142 followed by drug-free complete growth media for 4 days, three replicates per condition.
143 1.5×10^7 cells were used for each replicate for ribosome sequencing. Ribosome
144 footprints were isolated based on previous publications [25,26], and each RNA sample was spiked
145 with 24 fmol of the synthetic 28-nt RNA oligo 5'-AUGUAACACGGAGUCGACCCGCAACGCGA-3'.
146 rRNA depletion was performed using the Low Input RiboMinus™ Eukaryote System v2 (Thermo
147 Fisher A15027), and sequencing libraries were generated using the NEBNext® Small RNA Library
148 Prep Set for Illumina® (NEB E7330). Libraries were pooled and sequenced using NextSeq 500
149 High Output, single-end reads, 75 cycles. In parallel, RNA was extracted for total RNA
150 sequencing using the Direct-zol RNA Miniprep Kit (ZymoResearch R2050) or the miRneasy Mini
151 Kit (Qiagen 217004) according to manufacturer protocols, followed by rRNA depletion as above
152 and DNase-treatment. Sequencing libraries were prepared with the TruSeq Stranded Total RNA
153 LT or TruSeq Stranded Total RNA-seq Sample Prep Kit from Illumina and sequenced paired-end
154 for 6-hour and 72-hr, and single-end for 72-hour time points.
155 Trimmed reads from ribosome profiling and RNA sequencing were aligned to the hg38
156 reference genome using HISAT2 [27]. For ribosome profiling, reads longer than 30 nucleotides
157 were filtered out, and remaining reads were assembled to GENCODE v26 transcript annotations
158 using StringTie [28]. Ribosome profiling quantifications were normalized to mapped spike-in reads,
159 and RNA-seq reads were normalized to million mapped reads. Translational efficiency (TE) for
160 each gene was calculated by dividing the number of normalized ribosome footprint reads by the
161 number of normalized RNA sequencing reads. Differential TE was calculated using t-tests on
162 log2-transformed TE of three actD-treated replicates versus three DMSO-treated replicates.
163 Geneset enrichment analysis (GSEA) was performed using the fgsea package (v1.26.0) on log2-
164 fold change of TE using gene sets from MSigDB v7.1[17,29-31].
165

166 **CRISPR screen**

167

168 CRISPR knock-out screen was performed on WiT49 cells using the Human Brunello
169 CRISPR knockout pooled library, a gift from David Root and John Doench (Addgene 73178). The
170 plasmid library was propagated, verified for maintenance of representation, and transfected as
171 recommended [32]. The viral supernatant was transduced into 1.0×10^8 WiT49 cells, at
172 multiplicity of infection of 0.3. Forty-eight hours after transduction, the cells were selected with
173 0.5 µg/ml puromycin for 7 days. After selection, 3×10^7 transduced cells were collected as
174 transduction reference, and the rest were split into two groups. These remaining cells were
175 expanded and treated with either 2nM actD or DMSO for 4 days. The media was then replaced
176 in both conditions for a washout of 3 days without actD or DMSO. Following this, another 7-day
177 cycle (4 days actD or DMSO treatment followed by 3 days washout) was carried out. Finally,
178 genomic DNA was extracted using DNeasy Blood & Tissue Kit (Qiagen 69506), and a sequencing
179 library was prepared from genomically-integrated single guide RNA (sgRNA) sequences [32]. These
180 were gel-size selected and sequenced at ~2.4 million single-end reads each, 100-bp length.
181 Computational analysis of CRISPR screens was performed using the MAGeCKFlute
182 pipeline follow published guidelines [33]. In brief, we mapped reads using the command 'mageck
183 count', and we tested sgRNA knockout efficiency using the command 'mageck mle'.
184 Downstream analysis was performed using the FluteRRA function in the MAGeCKFlute R
185 package, with the 'mageck mle' output file as the input. To perform KEGG pathway enrichment
186 analysis, the 'mageck pathway' command was used with the KEGG gene set from the Molecular
187 Signatures Database (v7.1) [29].
188

189 **Western blot**

190 For the actD timecourse, WiT49 or 17.94 was seeded at ~30% confluency overnight. The
191 following day, without replacing the media, actD (or an equivalent volume of DMSO) was spiked
192 into the media to a final concentration of 2 nM, for 72-hour treatment. The next day, another
193 plate of WiT49 or 17.94 began 48-hour treatment with 2nM actD. We repeated this the
194 following day for the 24-hour treatment and 18-hour treatments. Upon completion of the
195 allotted incubation times, we collected cells for protein lysate extraction. For actD and BTZ *in*

196 *vitro* drug treatments, we seeded WiT49 or 17.94 at 20-30% confluency overnight. We then
197 treated cells with either 2nM actD alone, 8nM BTZ alone, 2nM actD + 8nM BTZ, or DMSO at
198 equivalent volume without changing media. After 48 hours of drug exposure, cells were
199 collected for protein lysate extraction.
200 Protein lysates were extracted from flash-frozen pellets with RIPA buffer (Sigma R0278),
201 supplemented with protease and phosphatase inhibitors (Invitrogen A32961), sonicated, and
202 quantified by BCA protein assay (Thermo Scientific 23227). Following denaturing SDS-PAGE and
203 transfer to PVDF or nitrocellulose membranes, blots were blocked with 5% bovine serum
204 albumin in tris-buffered saline with Tween-20. Primary antibodies used are as follows and were
205 diluted to 1:3,000 unless otherwise stated: Tubulin (Cell Signaling Technology 3873,
206 RRID:AB_1904178), GAPDH (Cell Signaling Technology 97166, RRID:AB_2756824), Caspase-3
207 (Cell Signaling Technology 9665, RRID:AB_2069872), cleaved Caspase-3 (Cell Signaling
208 Technology 9664, RRID:AB_2070042; 1:1,000), Caspase-7 (Cell Signaling Technology 12827,
209 RRID:AB_2687912), cleaved Caspase-7 (Cell Signaling Technology 8438, RRID:AB_11178377;
210 1:1,000), Caspase-9 (Cell Signaling Technology 9508, RRID:AB_2068620), cleaved Caspase-9 (Cell
211 Signaling Technology 7237, RRID:AB_10895832; 1:1,000), Cyclin D2 (Cell Signaling Technology
212 3741; RRID:AB_2070685), CDT1 (Cell Signaling Technology 8064, RRID:AB_10896851), Cyclin E1
213 Cell Signaling Technology 20808, RRID:AB_2783554), Cyclin A2 (Cell Signaling Technology
214 91500RRID:AB_3096041), PARP (Cell Signaling Technology 9532, RRID:AB_659884), cleaved
215 PARP (Cell Signaling Technology 5625, RRID:AB_10699459; 1:1,000), POMP (Cell Signaling
216 Technology 15141, RRID:AB_2798726), PSMA6 (Cell Signaling Technology 2459,
217 RRID:AB_2268879), PSMB1 (Invitrogen PA5-49648, RRID: AB_2635102; 1:5,000), PSMB2
218 (Proteintech 15154-1-AP, RRID:AB_2300322; 1:5,000), PSMB5 (Cell Signaling Technology 12919,
219 RRID:AB_2798061; 1:5,000), PSMD1 (Sigma SAB2104781, RRID:AB_10668741), RPL5 (Cell
220 Signaling Techonology 51345, RRID:AB_2799391), RPL7 (abcam ab72550, RRID:AB_1270391),
221 RPL11 (Cell Signaling Technology 18163, RRID:AB_2798794), RPL26 (Cell Signaling Technology
222 2065, RRID:AB_2146242), Total AKT (Cell Signaling Technology 9272, RRID:AB_329827),
223 Phospho-AKT (Ser473) (Cell Signaling Technology 4060, RRID:AB_2315049; 1:1,000), Total 4E-
224 BP1 (Cell Signaling Technology 9452, RRID:AB_331692), Phospho-4E-BP1 (Thr37/46) (Cell

225 Signaling Technology 2855, RRID:AB_560835; 1:1,000), Total P70-S6K1 (Cell Signaling
226 Technology 34475, RRID:AB_2943679), and Phospho- P70-S6K1 (Thr389) (Invitrogen 710095,
227 AB_2532559; 1:1,000). HRP-conjugated secondary antibodies used are Anti-Mouse IgG (Cell
228 Signaling Technology 7076, RRID:AB_330924; 1:10,000) or Anti-Rabbit IgG (Cell Signaling
229 Technology 7074, RRID:AB_2099233; 1:5,000).
230
231 ***In vitro* drug inhibition**
232
233 To quantify drug inhibitory activity, 1,000 cells per well were seeded in black-walled 96-
234 well plates at 100 µl/well. The following day, serial dilutions of actD (Sigma A1410), BTZ (Sigma
235 5043140001), or Rapamycin (Selleckchem S1039) were added in 3 replicates per dose. Vehicle
236 control was also included to yield equivalent final concentrations of DMSO (<0.1%) in all wells.
237 For synergy determination experiments, each drug of interest was serially diluted alone and
238 then mixed into a range of combinations. Each dose was then added onto the cells in triplicate.
239 After 72 hours, cell density was assayed by adding 20 µL 0.15 mg/ml resazurin in phosphate-
240 buffered saline in each well, including cell-free wells as background controls and drug-free wells
241 as normalization controls. After 1-4 hours at 37°C, fluorescence was measured using a
242 microplate reader with excitation set at 550 nm and emission at 590 nm. Combination
243 treatment effects were determined using the Loewe synergy model dose-response calculation
244 through Synergyfinder+ [34].
245
246 **Proteasome activity assay**
247
248 To measure proteasome enzymatic activity, we seeded 1,000 cells per well concurrently
249 in duplicate 96-well plates: one black-walled and one white-walled. The following day, the cells
250 were treated with each of the following conditions in quadruplicate with identical conditions in
251 both plates: 2nM actD, 2 nM actD + 1 mM MG-132 (Selleckchem S2619), 8 nM BTZ, 8 nM + 1
252 mM MG-132, DMSO, or DMSO + 1 mM MG-132. Wells without cells were used as background
253 controls. After 48 hours, the black-walled plate was used to determine cell viability as described

254 above. The white-walled plate was used to quantify proteasome enzymatic activity. We used
255 Proteasome-Glo™ Chymotrypsin-like Assay (Promega G8621) and calculated the proteasome
256 enzymatic activity in accordance with manufacturer recommendations. Briefly, after subtracting
257 background controls, we normalized each condition to viability based on the corresponding
258 wells in the black-walled plate to account for differences in cell density. We then subtracted the
259 normalized luminescence of each condition with MG-132 from the corresponding wells without
260 MG-132 to yield the viability-normalized luminescence attributable to proteasome activity.
261 Statistical significance was calculated using unpaired, two-tailed Student's T-test.
262
263
264 **Xenograft tumor models**
265
266 All experiments involving animals were reviewed, approved, and monitored for
267 compliance by the UT Southwestern Institutional Animal Care and Use Committee.
268 To generate xenografts, log growth-phase 17.94 cells or freshly-thawed cryopreserved
269 *TP53* mutated anaplastic Wilms tumor PDX line KT-53 [35] were injected subcutaneously into the
270 flanks of NOD *scid* gamma (NSG) mice in 1 part DPBS and 1 part Matrigel (Corning 354234) at 4
271 million 17.94 per 100 µl or 1.6 million KT-53 cells per 100 µl per mouse. Tumor growth was
272 measured once a week with calipers in two dimensions. Tumor volume was calculated by
273 dividing the product of the length and the square of the width by 2. Upon reaching the
274 thresholds of 150 mm^3 for 17.94 and 100 mm^3 for KT-53, mice were entered into one of four
275 treatment arms: actD only, BTZ only, both actD + BTZ and vehicle. Mice in the actD only and
276 actD+BTZ arms were dosed with actD (in 2.5% DMSO, 40% PEG300, 5% Tween-80, 52.5% saline)
277 once a week intraperitoneally (0.2 mg/kg for 17.94, 0.15 mg/kg for KT-53). Mice in the BTZ only
278 or actD+BTZ arms were dosed with BTZ (in 0.5% DMSO, 30% PEG300, 69.5% distilled deionized
279 water) once a week intravenously (0.2mg/kg). Mice in the vehicle arm received both solvents
280 once a week. Treatment continued until tumor volumes reached 1,500 mm^3. At the end of
281 therapy, tumors were harvested for histological processing. Statistical analyses for tumor
282 volume were performed by two-tailed Student's T-test for each pairwise comparison between

283 the four treatment arms. Kaplan-Meier survival curves were compared between each group by
284 log-rank test.
285
286 **IHC & TUNEL**
287
288 Two representative samples from each treatment arm were formalin-fixed, paraffin-
289 embedded, and sectioned at 4 µm thickness. These were used for immunohistochemistry (IHC)
290 and TUNEL assay.
291 For IHC, antibodies used were Ki-67 (Abcam ab15580, RRID:AB_443209, 1:1,000 for
292 primary) with anti-Rabbit HRP (Vector Laboratories Inc. MP-7451, RRID:AB_2631198 for
293 secondary). Each slide was photographed in at least four distinct 40x magnified fields of view
294 (Keyence Corporation). Numbers of total nuclei and DAB-positive nuclei in each field were
295 quantified using Fiji [36]. Non-tumor regions were omitted from quantification. Statistical analysis
296 was performed by unpaired two-tailed Student's t-test between each pair of treatment arms.
297 To measure apoptosis in tumor sections, we used Click-iT™ Plus TUNEL Assay kit
298 (Invitrogen C10617) according to the manufacturer recommendations and counterstained nuclei
299 with DAPI. Each tissue slide was photographed in at least four distinct 40x magnified fields of
300 view (Keyence Corporation). Numbers of total nuclei and TUNEL-positive nuclei and quantified
301 using Fiji [36]. Non-tumor regions were omitted from quantification. Statistical analysis was
302 performed by unpaired two-tailed Student's t-test between each pair of treatment arms.
303
304 **TARGET database reanalysis**
305
306 Tables of Wilms tumor RNA-seq counts and clinical annotation were downloaded from
307 the NCI TARGET[8] website on May 21, 2019. Protein-coding genes were identified based on
308 ENSEMBL v86 annotations. Differential expression analysis for DAWT versus FHWT was
309 performed with DESeq2 (v1.40.2), followed by gene set enrichment analysis using fgsea
310 (v1.26.0) based on MSigDB v7.1 gene sets [17,31,37].

311 We compared outcomes for these patients according to expression of proteasome
312 enzymatic subunits in cBioportal [38,39]. Specifically, we obtained RNA-seq RPKM z-scores for each
313 gene of interest compared to tumors that are diploid for that gene. For patients with multiple
314 samples, the primary tumor sample was used. Based on expression of *PSMB5*, *PSMB6*, and
315 *PSMB7*, tumors with at least one gene z-score ≥ +1 were categorized as "PSMs high", while
316 those with at least one gene z-score ≤ -1 were categorized as "PSMs low". Samples with z-scores
317 between -1 and +1 for all three genes were categorized as "PSMs medium". Those with one
318 gene z-score ≥ +1 and another gene z-score ≤ -1 were omitted (n=8). Log-rank tests were used
319 to compare survival curves.
320
321 **Data availability**
322
323 Ribosome profiling and accompanying RNA-seq data from WiT49 are deposited in the
324 NCBI GEO database under accession GSE270330.

325 **RESULTS**

326

327 **Actinomycin alters the translational landscape of anaplastic Wilms tumor cells**

328

329 ActD blocks rRNA transcription at nanomolar doses and mRNA transcription at
330 micromolar doses [18]. To examine whether actD is effective at nanomolar doses in anaplastic
331 Wilms tumor, we measured 72-hour actD sensitivity in two anaplastic Wilms tumor cell lines,
332 WiT49 and 17.94 (Supplementary Figure S1B). For these cell lines, we measured IC50 to be 1.3
333 and 2.2 nM, respectively. Next, we confirmed that 2 nM actD reduces levels of 45s pre-rRNA
334 and 18s mature rRNA in both cell lines (Supplementary Figure S1C). This results in decreased
335 overall protein synthesis, consistent with specific impairment of Pol I activity (Supplementary
336 Figure S1D and Figure 1A).

337 Thus, to understand how actD affects protein levels and cellular functions in Wilms
338 tumor, we next performed three assays in parallel: ribosome profiling, to identify preferentially
339 translated transcripts; reverse-phase protein arrays (RPPA), to identify differences in protein
340 levels and post-translational modifications; and a CRISPR dropout screen, to identify targetable
341 vulnerabilities.

342 First, to ascertain preferentially translated transcripts, we performed ribosome profiling
343 in WiT49 cells treated with actD or vehicle control at 6 hours, 72 hours, and two weeks. At each
344 timepoint, we performed ribosome profiling to quantify gene-level differences in translational
345 efficiency in actD- versus vehicle-treated cells. To confirm the expected effect of depleting
346 ribosomes, we examined the locations of the ribosome footprint edges in metagene plots
347 around translation start sites (Supplementary Figure S2A). As expected, in both DMSO- and
348 actD-treated cells, there were essentially no detectable reads in 5' untranslated regions (UTRs),
349 while coding sequences exhibit a trinucleotide periodicity, reflecting the reading frame of
350 elongating ribosomes. In DMSO-treated cells, the left edge of ribosome footprints accumulated
351 just upstream of translation start sites, which reflects pausing of the ribosome at the initiation
352 site, as expected for normal conditions. In actD-treated cells, however, the initiation site peak
353 was blunted, suggesting that when ribosomes are depleted, the ribosomes that remain spend

354 less time paused at initiation. For all durations of treatment, actD appeared to have minimal
355 effect on the transcriptome (Supplementary Figure S2B). On the other hand, ribosome
356 footprints revealed gross perturbation of translational landscapes by actD (Supplementary
357 Figure S2C). After two weeks of intermittent actD dosing, cells appear to return to a new steady
358 state with globally reduced translation.

359 We next compared the translational efficiency of each gene in actD-treated cells at 6 and
360 72 hours, and we connected preferentially translated genes (Supplementary Tables S1, S2) into
361 Kyoto Encyclopedia of Genes and Genomes (KEGG) pathways using GSEA. The most enriched
362 KEGG pathway by translational efficiency at both timepoints was KEGG_RIBOSOME, which is
363 composed of RPs and genes that regulate ribosome biosynthesis (Figures 1B, 1C; Supplementary
364 Figures S3A, S3B; Supplementary Tables S3, S4). This is consistent with reports that RPs are
365 unstable when actD depletes rRNA, and a decrease in ribosomes leads to feedback signaling to
366 upregulate translation of RPs via the mTORC1 pathway [40,41]. KEGG_PROTEASOME was the only
367 other gene set in the top five most preferentially translated gene sets at both timepoints (Figure
368 1B, 1C; Supplementary Figure S3C, S3D; Supplementary Tables S3, S4). On the other hand, the
369 most downregulated gene sets at 6 hours entailed nucleotide turnover, which led to a depletion
370 of cell cycle genes at 72 hours (Figure 1D, 1E; Supplementary Tables S3, S4).

371 Next, we used a genome-wide CRISPR screen to identify therapeutic vulnerabilities in
372 cells with intermittent actD or DMSO for 14 days. We again used KEGG pathways to categorize
373 dependency genes (Figure 1F; Supplementary Table S5). Here, we again found enrichment for
374 pathways related to protein turnover, including KEGG_PROTEASOME, as well as nucleic acid
375 turnover and cell cycle.

376 Thirdly, since actD regulates protein synthesis, we also performed RPPA on WiT49 cells
377 treated with actD or DMSO for 72 hours to understand how actD affects protein levels and post-
378 translational modifications (Figure 1G; Supplementary Table S6). We found an increase in
379 phosphorylation of some components of the mTORC1 signaling pathway, which mediates the
380 feedback signaling to upregulate translation of RPs in the setting of rRNA depletion [41]. On the
381 other hand, cell cycle markers such as CDT1, CDC6, and phosphorylated RB1 were depleted in

382 actD-treated cells. This is consistent with depletion of cell cycle gene sets in ribosome profiling
383 at 72 hours.
384
385 **mTORC1 inhibition does not sensitize Wilms tumor cells to actinomycin D**
386 Based on phosphorylation of mTORC1 signaling intermediates in RPPA and prior interest
387 in mTORC1 signaling in Wilms tumor [42,43], we next investigated how actD affected mTORC1
388 signaling in WiT49 and a second anaplastic Wilms tumor cell line, 17.94. Using Western blots,
389 we confirmed that actD induced phosphorylation of AKT and 4E-BP1 in WiT49 and 17.94 cells
390 (Supplementary Figure S3E). (The phosphorylation of another mTORC1 target, p70S6K, was not
391 clearly upregulated.) We treated WiT49 and 17.94 with rapamycin at doses up to 100 µM and
392 found that this drug confers a more cytostatic rather than cytotoxic effect (Supplemental Figure
393 S3F). We also measured cell viability in combinations of actD and the mTORC1 inhibitor
394 rapamycin using the Loewe independence model (Supplementary Figure S3G). However, the
395 interaction did not show synergy at the serum concentrations of these drugs typically achieved
396 in patients. In other words, mTORC1 inhibition with rapamycin did not appear to sensitize Wilms
397 tumor cells to actD.
398
399 **ActD induces proteotoxic stress and cell cycle arrest in anaplastic Wilms tumor cells**
400 One effect of mTORC1 signaling is to upregulate translation of RPs [44], and
401 KEGG_RIBOSOME was the most enriched gene set in actD-treated cells. Although actD induced
402 preferential translation of RPs, we found that actD treatment in fact reduced total protein levels
403 of multiple RPs in both WiT49 and 17.94 (Figure 2A). This is consistent with prior reports that
404 excess RP subunits are unstable without rRNA and are degraded by the proteasome to maintain
405 appropriate RP:rRNA stoichiometry [40,45,46]. For some RPs, this effect was partially rescued by the
406 proteasome inhibitor bortezomib (BTZ).
407 On the other hand, preferential translation of proteasome components led to their
408 accumulation. When we exposed WiT49 and 17.94 to actD for up to 72 hours, both cell lines
409 exhibited an appreciable increase in proteasome complex subunits PSMD1 (also known as
410 P112), PSMA6 (subunit α1), PSMB1 (β6), PSMB2 (β4), and PSMB5 (β5), as well as the molecular

411 chaperone for proteasome assembly, POMP, at one or more timepoints (Figure 2B). These
412 increases in protein levels of proteasome components corresponded to increased proteasome
413 chymotrypsin-like enzymatic activity in both cell lines, which was blunted by bortezomib (Figure
414 2C).

415 Because actD caused preferential translation of proteasome subunits, we next examined
416 how WiT49 and 17.94 respond to proteasome inhibition. These two cell lines were sensitive to
417 BTZ alone at nanomolar concentrations, in the range of serum levels typically achieved in
418 patients [47,48] (Figure 3A). Furthermore, in this dose range, actD and BTZ synergistically inhibited
419 both WiT49 and 17.94 (Figure 3B). In other words, BTZ could be a way to enhance or restore
420 actD sensitivity in anaplastic Wilms tumors.

421 BTZ has previously been shown to trigger cell death, cell cycle arrest, and autophagy in
422 cancer cell lines [49-54]. To understand whether actD and BTZ could cooperate in Wilms tumor, we
423 treated WiT49 and 17.94 with actD and/or BTZ for 48 hours. In both cell lines, actD alone
424 reduces cell cycle markers, including chromatin licensing and DNA replication factor 1 (CDT1),
425 cyclin D2, cyclin E1, and cyclin A2 (Figure 3C) [55-57]. These cell cycle regulators are synthesized
426 and degraded in each turn of the cell cycle [58,59]. These support our findings from CRISPR screen
427 and protein arrays, which showed that actD induced a dependency on cell cycle genes and led
428 to a fall in cell cycle markers (Figures 1F, 1G) Together, these results suggest that the proteotoxic
429 stress caused by actD triggers cell cycle arrest.

430 In addition to impaired cell cycle progression, use of the proteasome inhibitor BTZ
431 resulted in the accumulation of apoptotic markers in both cell lines (Figure 3C) [60-63]. ActD alone
432 induced cleaved caspase-7 and PARP in 17.94 cells, but even more so in BTZ alone and
433 combination treatment for 17.94 and for WiT49. The combination of these effects supports the
434 potential for using actD and BTZ to target anaplastic Wilms tumors.

435

436 **Combined treatment of actinomycin D and bortezomib in Wilms tumor xenografts suppresses**
437 **growth *in vivo***

438 We next examined the effect of combining BTZ with actD against two anaplastic Wilms
439 tumor lines *in vivo*: cell line-derived xenografts from 17.94 and the *TP53* mutated patient-

440 derived xenograft (PDX) line KT-53 [35,64]. We implanted both lines into NSG mice and treated
441 them with vehicle only, actD, BTZ, or both. We found that combination treatment significantly
442 reduced tumor volume and conferred a significant survival advantage for mice bearing KT-53
443 xenografts compared to the other three arms (Figure 4A, 4B, Supplementary Figure S4A).
444 Similarly, 17.94 xenografts treated with the combination of actD and BTZ were significantly
445 smaller than those who received vehicle control or BTZ alone (Figure 4C, 4D, Supplementary
446 Figure S4B). (Although it did not reach statistical significance, tumor volume in the combination
447 treatment cohort was also smaller than the actD-only arm.)
448 Based on the effects of actD and BTZ on cell cycle and apoptosis we had observed *in*
449 *vitro*, we next measured cell cycle and apoptosis markers in these subcutaneous tumors. We
450 used immunohistochemistry for Ki-67 as a marker of proliferation and TUNEL assay as a marker
451 of apoptosis. In both lines, tumors from combination-treated mice had a statistically significant
452 reduction in proliferation compared to vehicle or BTZ alone (Figure 4E, Supplemental Figure
453 S4C, S4D). Similarly, in both lines, combination treatment yielded significantly more apoptosis
454 than vehicle and actD alone (Figure 4F, Supplemental Figure S4E, S4F). Taking these into
455 consideration, we find that the compounding effects of adding BTZ to actD could be a powerful
456 approach to targeting anaplastic Wilms tumor cells.
457
458 **Proteasome subunit expression levels correlate with outcome**
459 Lastly, we examined expression of proteasome genes in publicly available RNA-seq data
460 from 42 DAWT and 83 relapsed FHWT samples generated by the NCI Therapeutically Applicable
461 Research to Generate Effective Treatments (TARGET) project [8]. Compared to FHWT, the single
462 most enriched KEGG gene set in DAWT was KEGG_PROTEASOME (Figure 5A, Supplementary
463 Figure S5A, Supplementary Table S7). Similarly, two of the three most enriched Reactome gene
464 sets were related to APC/C-mediated degradation of cell cycle proteins, suggesting that
465 proteasomal degradation promotes proliferation in DAWT by degrading proteins in each cell
466 cycle (Figure 5B, Supplementary Figure S5B, Supplementary Table S8).
467 Next, we examined whether expression of proteasome subunits correlated with
468 outcome in Wilms tumor. We stratified FHWT and DAWT patients into three categories based on

469 high, medium, or low expression of the enzymatic proteasome subunits *PSMB5* (β5), *PSMB6*
470 (β1), and *PSMB7* (β2). Among relapsed FHWT patients, who usually receive actD-based
471 chemotherapy regimens at diagnosis, proteasome-high patients fared far worse than
472 proteasome-low or proteasome-medium patients (Figure 5C). Among DAWT patients, who do
473 not usually receive actD-based therapy regimens, the relationship between proteasome
474 expression and outcome was less evident; proteasome-medium patients fared worse than
475 proteasome-low patients, but proteasome-high patients were not significantly different from
476 proteasome-medium or -low [8,38,39] (Figure 5D). In the entire Wilms tumor cohort, nevertheless,
477 higher proteasome subunit expression correlated with worse survival (Supplementary Figure
478 S5C). Together, these data suggest that proteasome subunit levels may underlie some of the
479 clinical differences between DAWT and FHWT, and that FHWT with high proteasome subunit
480 levels are as aggressive as DAWT. Proteasome inhibition could benefit both subgroups.

481 **DISCUSSION**

482

483 Developments in Wilms tumor research have illuminated the mutational, epigenetic,
484 mRNA, and miRNA expression landscapes of these tumors, yet relevant targetable
485 vulnerabilities remain elusive [8,65-69]. Anaplastic Wilms tumors exhibit relative resistance to
486 conventional chemotherapy, including actD, and little is known about why anaplastic Wilms
487 tumors are resistant to actD or how to overcome such resistance. Furthermore, despite its
488 widespread use, little is known about how actD influences the translational landscape of cancer.
489 Understanding the mechanisms underlying these effects and their consequences could
490 potentially uncover targetable vulnerabilities in relatively chemo-refractory anaplastic Wilms
491 tumors, which could enhance outcomes while minimizing off-target toxicities in survivors.
492 Through several orthogonal approaches, our work reveals that actD disrupts protein
493 homeostasis in Wilms tumor and suggests proteasome inhibition as a potential targeted therapy
494 for inducing actD sensitivity in anaplastic Wilms tumors.

495 Protein homeostasis involves a synchronized and responsive balance between protein
496 synthesis and degradation, which are both affected by actD. Since protein synthesis is energy-
497 intensive, particularly in rapidly proliferating cancers where proteins like cyclins are
498 continuously synthesized and degraded, maintaining protein homeostasis is crucial to ensure
499 optimal levels of amino acids and other nutrients for growth [70-72]. Blocking protein synthesis
500 with actD mimics amino acid starvation, leading cells to upregulate Akt/mTORC1 signaling,
501 which in turn increases the translation of ribosomal protein (RP) genes [44,73-75]. Although the
502 mTOR pathway is a potential therapeutic target in Wilms tumor and other cancers [76-78], the
503 combination of actD and rapamycin did not consistently show synergy *in vitro* for either cell line,
504 and rapamycin alone only exhibited a cytostatic effect. Our cells were in nutrient-rich media
505 which may be compounding to the variables that dictate the effect of rapamycin [77,79], and our
506 results do not rule out the possibility that other mTOR signaling inhibitors could still have
507 potential.

508 On the other hand, based on our finding that proteasome subunits were preferentially
509 translated after actD exposure, we found that proteasome inhibition with BTZ sensitizes cells to
510 actD *in vitro* and *in vivo*. The proteasome is upregulated in response to proteotoxic stresses

511 [45,46,80], and Akt/mTORC1 activates proteasome subunit expression via *Nrf1/NFE2L1* [81-84] to
512 enhance the intracellular amino acid pool and the unfolded protein response. BTZ was the first
513 proteasome inhibitor approved by the United States Food and Drug Administration [85-87], and it
514 has been tested in pediatric cancer patients [47,88,89]. However, other than a study showing a lack
515 of cross-resistance between actD and BTZ in gliobastoma [90], no published studies have explored
516 combinatorial treatment of actD and BTZ to our knowledge. Compellingly, for both KT-53 and
517 17.94, combination treatment reduced proliferative cells and increased apoptosis. In particular,
518 our study on KT-53 recapitulated a previously demonstrated insensitivity to actD [35], which we
519 found could be overcome by BTZ. Thus, our findings indicate that the combined use of actD and
520 BTZ can be a promising strategy for combating therapy resistance in anaplastic Wilms tumors.
521 We demonstrated that actD impairs cell cycle progression *in vitro* and *in vivo*, which we
522 attribute to dysregulated proteostasis [15,91,92]. Normally, D-type cyclin levels accumulate in
523 response to mitogenic signaling, promoting the transcription of S-phase genes such as E-type
524 cyclins and chromatin licensing and DNA replication factor 1 (CDT1) [58,93,94]. Consistent with our
525 RPPA in WIT49, we observed in both cell lines that actD reduces Cyclin D2, Cyclin E1, and CDT1
526 levels, suggesting that actD prevents transition to S-phase, when cyclin A is produced. On the
527 other hand, these proteins are normally targeted for proteasomal destruction by the SKP1-
528 CUL1-F-boc protein (SCF) ubiquitin ligase [95], and indeed, we found that BTZ caused them to
529 accumulate. Moreover, BTZ treatment induced apoptosis *in vitro* and *in vivo*, consistent with
530 studies on other cancer cell lines [49-54].
531 In the TARGET cohort [8], we found that higher levels of proteasome gene expression
532 correlate with anaplastic histology and with poor outcome among favorable-histology Wilms
533 tumors. Studies across other types of cancer show that the association of proteasome activity
534 with prognosis is context-specific [96]. Lower expression of proteasome subunit genes was
535 associated with reduced survival in head and neck squamous cell carcinoma [97], while studies in
536 breast cancer, glioma, and hepatocellular carcinoma found that higher expression of
537 proteasome subunit genes is associated with worse survival [98-100]. To our knowledge, this is the
538 first study to correlate proteasome expression with worse outcome in Wilms tumor. Anaplastic
539 Wilms tumors are strongly associated with P53 mutation [7,8], and P53 mutation is known to

540 contribute to proteasome subunit overexpression [101]. Taken together with our experimental
541 data, these data provide a potential molecular basis to explain the divergent efficacy of actD in
542 FHWT versus DAWT.
543 To our knowledge, this is the first study to explore the translational landscape of actD
544 treatment and highlight the importance of the proteasome in Wilms tumor. Through *in vitro* and
545 *in vivo* models, we propose a model of protein homeostasis-dependent actD sensitivity
546 (Supplementary Figure S5D). Use of actD impairs ribosome biogenesis and cell cycle
547 progression while upregulating proteasome activity. Higher proteasome capacity may help
548 Wilms tumor cells escape chemotherapeutics like actD, and this effect may be reversed with
549 proteasome inhibition. For these reasons, proteasome inhibition could improve outcomes in
550 both favorable-histology and diffusely anaplastic Wilms tumor. Repurposing widely used drugs
551 like BTZ could allow for an accelerated path to clinical translation. This strategy could improve
552 treatment not only for Wilms tumor, but also for other tumors where actD is used, such as
553 rhabdomyosarcoma and Ewing sarcoma.
554

ACKNOWLEDGMENTS

This work was supported by funds from the Pablove Foundation (to P.D.B.T.); Alex's Lemonade Stand Foundation (to K.S.C.); Cancer Prevention and Research Institute of Texas (RP180805 to L.X., RR180071 to K.S.C.); and National Cancer Institute (K08CA207849 to K.S.C., R21CA259771 and P30CA142543 to L.X., and Cancer Center Support Grant P30CA142543). This research used computational resources provided by the BioHPC supercomputing facility in the Lyda Hill Department of Bioinformatics at UT Southwestern, which is supported by Cancer Prevention and Research Institute of Texas (RP150596). The Functional Proteomics Reverse Phase Protein Array Core was supported in part by The University of Texas MD Anderson Cancer Center, P30CA016672 and R50CA221675.

574 **FIGURE LEGENDS**

575

576 **Figure 1. ActD disrupts protein homeostasis in anaplastic Wilms tumor cells**

577 **(A)** Quantification of protein synthesis assay (OPP incorporation) in WiT49 cells treated with 48
578 and 72 hours of 2nM actD or vehicle DMSO.

579 **(B,C)** Most enriched KEGG gene sets in ribosome profiling of actD- vs. DMSO-treated WiT49
580 after 6 hours **(B)** or 72 hours **(C)**.

581 **(D,E)** Most depleted KEGG gene sets in ribosome profiling of actD- vs. DMSO-treated WiT49
582 after 6 hours **(D)** or 72 hours **(E)**.

583 **(F)** GSEA of genome-wide CRISPR knockout library screen reveals top 10 most significant KEGG
584 canonical pathways that sensitize WiT49 to actD pathways, ranked by p-value. Highlighted are
585 the KEGG_PROTEASOME and KEGG_CELL_CYCLE, where the dotted line represents p-value at
586 0.05.

587 **(G)** Heatmap displaying results from RPPA of actD- versus DMSO-treated WiT49. Normalized,
588 log2-transformed, median-centered values from validated antibodies with standard deviation
589 over 0.1 are shown here.

590

591 **Figure 2. ActD promotes proteasome level and activity in anaplastic Wilms tumor cells**

592 **(A)** Western blots for ribosomal protein subunits RPL5, RPL7, RPL11, and RPL26 in WiT49 and
593 17.94 following 48-hour treatment of DMSO, 2nM actD, 8nM BTZ, or 2nM ActD + 8nM BTZ.

594 **(B)** Protein levels of proteasome subunits PSMA6 (α1), PSMB1 (β6), PSMB2 (β4), PSMB5 (β5),
595 and PSMD1 (P112), and POMP in WiT49 and 17.94 following 18-, 24-, 48-, and 72-hour 2nM
596 actD treatment versus vehicle (DMSO).

597 **(C)** Quantification of relative proteasome-specific chymotrypsin-like activity in WiT49 and 17.94
598 cells following 24 hours of DMSO versus 2nM actD, 8nM BTZ, or 2nM actD + 8nM BTZ
599 treatments (Student's t-test p-value versus vehicle: *<0.05, ** <0.01, ****<0.0001).

600

601 **Figure 3. BTZ sensitizes anaplastic Wilms tumor cell lines to actD *in vitro***

602 **(A)** BTZ kill curves for WiT49 and 17.94 with IC50 values indicated (four-point regression line
603 with shaded region representing 95% confidence interval).
604 **(B)** Heat maps of Loewe synergy scores for combinations of actD and BTZ in WiT49 and 17.94
605 cells.
606 **(C)** Effect of 48-hour treatment WiT49 and 17.94 cells with DMSO, actD, BTZ, and combination
607 actD + BTZ on cell cycle and apoptosis markers by Western blot.
608
609 **Figure 4. BTZ sensitizes subcutaneous anaplastic Wilms tumor xenografts to actD**
610 **(A)** Subcutaneous tumor volumes of NSG mice bearing KT-53 xenografts treated with vehicle,
611 actD, BTZ, and combination actD + BTZ (Student's t-test of endpoint volumes of combination
612 versus vehicle or actD only: * <0.05).
613 **(B)** Kaplan-Meier survival curves for KT-53 tumor-bearing mice treated with vehicle, actD only,
614 BTZ only, and combination (log-rank test versus vehicle ** <0.01).
615 **(C)** Subcutaneous tumor volumes of NSG mice bearing 17.94 xenografts treated with vehicle,
616 actD only, BTZ only, and combination (Student's t-test of endpoint volumes of combination
617 versus vehicle: ***<0.001).
618 **(D)** Kaplan-Meier survival curves for 17.94 tumor-bearing mice treated with vehicle, actD only,
619 BTZ only, and combination.
620 **(E,F)** Quantification of Ki-67 positive nuclei **(E)** and TUNEL positive nuclei **(F)** in in KT-53 and
621 17.94 subcutaneous tumors treated with vehicle, actD only, BTZ only, or combination actD + BTZ
622 (Student's t-test p-value versus vehicle unless otherwise indicated: * <0.05, **<0.01, ***<0.001,
623 ****<0.0001).
624
625 **Figure 5. RNA expression of proteasome genes in TARGET favorable and anaplastic histology**
626 **Wilms tumors**
627 **(A)** Top KEGG pathways enriched in RNA-seq of DAWT versus FHWT.
628 **(B)** Top reactome pathways enriched in RNA-seq of DAWT versus FHWT.

629 **(C,D)** Overall survival of tumors stratified according to expression of proteasome enzymatic
630 subunit genes *PSMB1, PSMB2, PSMB5* among patients with favorable histology tumors **(C)** or
631 anaplastic histology **(D)**. (Log Rank test p-value: *<0.05, ** 0.01)
632
633
634

635 **SUPPLEMENTARY FIGURES**

636

637 **Supplementary Figure S1. ActD alters global translation in WiT49 anaplastic Wilms tumor cells**

638 **(A)** Diagram of the effect of actD on Wilms tumor cells at the translational level. ActD depletes

639 fully-formed ribosomes and reduces translational capacity. The reduced ribosomes are

640 distributed unevenly, resulting in an altered translational landscape. Identification of the

641 ribosomal footprints by ribosome profiling provides a snapshot of transcripts actively

642 undergoing translation.

643 **(B)** ActD kill curves for anaplastic Wilms Tumor cell lines WiT49 and 17.94 with IC50 values

644 indicated (four-point regression line with shaded region representing 95% confidence interval).

645 **(C)** Levels of 45s pre-rRNA and 18s mature rRNA in anaplastic Wilms tumor cell lines WiT49 and

646 17.94, quantified by qPCR following actD treatment for 6 and 24 hours.

647 **(D)** Micrographs of protein synthesis assay. Red fluorescence measures OPP incorporation

648 relative to total area of WiT49 cells treated with 48 and 72 hours of 2nM actD or vehicle DMSO.

649

650 **Supplementary Figure S2. Ribosome profiling metrics in actD-treated WiT49.**

651 **(A)** Position of left edge of ribosome footprints relative to translation initiation site (0), on the

652 top 30% most abundant transcripts, in DMSO and actD samples at 72 hours. Peak position

653 highlighted in red.

654 **(B,C)** Log2-transformed counts aligning to each gene, by RNA-seq **(B)** and translation efficiency

655 by ribosome profiling **(C)** after 6-hour, 72-hour, and 2-week treatments of WiT49 with actD (y-

656 axes) versus DMSO (x-axes).

657

658 **Supplementary Figure S3. ActD induces translation of ribosome and proteasome subunits and**

659 **upregulates Akt/mTOR signaling.**

660 **(A,B)** KEGG_ RIBOSOME pathway enrichment plots after 6 hours (A) and 72 hours (B) of

661 exposure to actD versus DMSO. (NES, Normalized Enrichment Score)

662 **(C,D)** KEGG_ PROTEASOME pathway enrichment plots after 6 hours (C) and 72 hours (D) of

663 exposure to actD versus DMSO. (NES, Normalized Enrichment Score)

664 **(E)** Changes in phosphorylation of Akt/mTOR signaling components visualized by western blot in
665 WiT49 and 17.94 following 2nM actD treatment versus vehicle (DMSO).
666 **(F)** Rapamycin kill curves for anaplastic Wilms Tumor cell lines WiT49 and 17.94 (four-point
667 regression line with shaded region representing 95% confidence interval)
668 **(G)** Heat maps of Loewe synergy scores for combinations of actD and rapamycin in WiT49 and
669 17.94 cells.
670

671 **Supplementary Figure S4. Bortezomib enhances cytotoxicity of actinomycin D in anaplastic**
672 **Wilms tumor xenografts.**
673 **(A,B)** Low-power and high-power H&E images of **(A)** KT-53 and **(B)** 17.94 subcutaneous tumors
674 (Black bar = 1.0 mm; Blue Bar =100 µm)
675 **(C, D)** High-power photomicrographs of Ki-67 immunohistochemistry of KT-53 (Bar =100 µm) **(C)**
676 and 17.94 **(D)**.
677 **(E, F)** High-power photomicrographs of TUNEL stain of KT-53 (Bar =100 µm) **(E)** and 17.94 **(F)**.
678

679 **Supplementary Figure S5. Enrichment for proteasome gene sets in anaplastic Wilms tumor.**
680 **(A,B)** GSEA plot showing enrichment for KEGG_PROTEASOME **(A)** and
681 REACTOME_APC_C_MEDIATED_DEGRADATION_OF_CELL_CYCLE_PROTEINS **(B)** in anaplastic
682 Wilms tumor vs. favorable-histology Wilms tumors in TARGET dataset.
683 **(C)** Overall survival of Wilms tumors, regardless of histology, stratified according to expression of
684 proteasome enzymatic subunit genes *PSMB1, PSMB2, PSMB5* among patients (Log rank test p-
685 value: *<0.05, *** 0.001).
686 **(D)** Model for effect of actinomycin D on protein homeostasis in Wilms tumor cells.
687
688
689
690

691 **SUPPLEMENTARY TABLES**

692

693 **Supplementary Table S1.** Average log2-transformed translational efficiency for WiT49 in 6-hour
694 actD versus DMSO treatments derived from ribosome profiling sequencing.

695

696 **Supplementary Table S2.** Average log2-transformed translational efficiency for WiT49 in 72-
697 hour actD versus DMSO treatments derived from ribosome profiling sequencing.

698

699 **Supplementary Table S3.** GSEA of translationally enriched KEGG pathways for WiT49 6-hour
700 actD versus DMSO treatments from ribosome profiling sequencing.

701

702 **Supplementary Table S4.** GSEA of translationally enriched KEGG pathways for WiT49 72-hour
703 actD versus DMSO treatments from ribosome profiling sequencing.

704

705 **Supplementary Table S5.** KEGG pathway enrichment summary table from Mageck-Flute
706 pathway output.

707

708 **Supplementary Table S6.** Normalized, log2-transformed, median-centered RPPA values of
709 validated antibodies from WiT49 cells treated with actD or DMSO.

710

711 **Supplementary Table S7.** GSEA of enriched KEGG pathways in DAWT versus FHWT.

712

713 **Supplementary Table S8.** GSEA of enriched Reactome pathways in DAWT versus FHWT.

714

715 **REFERENCES**
716
717
718

719 1 Howlader N, N. A., Krapcho M, Miller D, Brest A, Yu M, Ruhl J, Tatalovich Z, Mariotto A,
720 Lewis DR, Chen HS, Feuer EJ, Cronin KA (eds). . *SEER Cancer Statistics Review, 1975-2018,*
721 *National Cancer Institute*, <https://seer.cancer.gov/csr/1975_2018/, > (2018).
722 2 Termuhlen, A. M. *et al.* Twenty-five year follow-up of childhood Wilms tumor: a report
723 from the Childhood Cancer Survivor Study. *Pediatr Blood Cancer* **57**, 1210-1216 (2011).
724 https://doi.org:10.1002/pbc.23090
725 3 Ehrlich, P. *et al.* Results of the First Prospective Multi-institutional Treatment Study in
726 Children With Bilateral Wilms Tumor (AREN0534): A Report From the Children's
727 Oncology Group. *Ann Surg* **266**, 470-478 (2017).
728 https://doi.org:10.1097/SLA.0000000000002356
729 4 Groenendijk, A. *et al.* Prognostic Factors for Wilms Tumor Recurrence: A Review of the
730 Literature. *Cancers (Basel)* **13** (2021). https://doi.org:10.3390/cancers13133142
731 5 Brok, J. *et al.* Unmet needs for relapsed or refractory Wilms tumour: Mapping the
732 molecular features, exploring organoids and designing early phase trials - A collaborative
733 SIOP-RTSG, COG and ITCC session at the first SIOPE meeting. *Eur J Cancer* **144**, 113-122
734 (2021). https://doi.org:10.1016/j.ejca.2020.11.012
735 6 Daw, N. C. *et al.* Activity of Vincristine and Irinotecan in Diffuse Anaplastic Wilms Tumor
736 and Therapy Outcomes of Stage II to IV Disease: Results of the Children's Oncology
737 Group AREN0321 Study. *Journal of clinical oncology : official journal of the American*
738 *Society of Clinical Oncology* **38**, 1558-1568 (2020). https://doi.org:10.1200/JCO.19.01265
739 7 Ooms, A. H. *et al.* Significance of TP53 Mutation in Wilms Tumors with Diffuse Anaplasia:
740 A Report from the Children's Oncology Group. *Clinical cancer research : an official*
741 *journal of the American Association for Cancer Research* **22**, 5582-5591 (2016).
742 https://doi.org:10.1158/1078-0432.CCR-16-0985
743 8 Gadd, S. *et al.* A Children's Oncology Group and TARGET initiative exploring the genetic
744 landscape of Wilms tumor. *Nature genetics* **49**, 1487-1494 (2017).
745 https://doi.org:10.1038/ng.3940
746 9 Macmahon, H. E., Bedizel, M. & Ellis, C. A. Vincristine (Leurocristine) Sulfate in the
747 Treatment of Children with Metastatic Wilms' Tumor. Pediatric Division, Southwest
748 Cancer Chemotherapy Group. *Pediatrics* **32**, 880-887 (1963).
749 10 Windmiller, J., Berry, D. H., Haddy, T. B., Vietti, T. J. & Sutow, W. W. Vincristine sulfate in
750 the treatment of neuroblastoma in children. *Am J Dis Child* **111**, 75-78 (1966).
751 https://doi.org:10.1001/archpedi.1966.02090040111014
752 11 Gaspar, N. *et al.* Ewing Sarcoma: Current Management and Future Approaches Through
753 Collaboration. *Journal of clinical oncology : official journal of the American Society of*
754 *Clinical Oncology* **33**, 3036-3046 (2015). https://doi.org:10.1200/JCO.2014.59.5256
755 12 Miwa, S. *et al.* Recent Advances and Challenges in the Treatment of
756 Rhabdomyosarcoma. *Cancers (Basel)* **12** (2020).
757 https://doi.org:10.3390/cancers12071758

13 D'Angio, G. J. The National Wilms Tumor Study: a 40 year perspective. *Lifetime Data Anal* **13**, 463-470 (2007). https://doi.org:10.1007/s10985-007-9062-0

14 Veal, G. J. *et al.* Pharmacokinetics of dactinomycin in a pediatric patient population: a United Kingdom Children's Cancer Study Group Study. *Clinical cancer research : an official journal of the American Association for Cancer Research* **11**, 5893-5899 (2005). https://doi.org:10.1158/1078-0432.CCR-04-2546

15 Walsh, C. *et al.* Development of a physiologically based pharmacokinetic model of actinomycin D in children with cancer. *Br J Clin Pharmacol* **81**, 989-998 (2016). https://doi.org:10.1111/bcp.12878

16 Perry, R. P. Selective effects of actinomycin D on the intracellular distribution of RNA synthesis in tissue culture cells. *Experimental Cell Research* **29**, 400-406 (1963).

17 Subramanian, A. *et al.* Gene set enrichment analysis: a knowledge-based approach for interpreting genome-wide expression profiles. *Proc Natl Acad Sci U S A* **102**, 15545-15550 (2005). https://doi.org:10.1073/pnas.0506580102

18 Schöfer, C., Weipoltshammer, K., Almeder, M., Muller, M. & Wachtler, F. Redistribution of ribosomal DNA after blocking of transcription induced by actinomycin D. *Chromosome Res* **4**, 384-391 (1996). https://doi.org:10.1007/BF02257274

19 Mills, E. W. & Green, R. Ribosomopathies: There's strength in numbers. *Science* **358** (2017). https://doi.org:10.1126/science.aan2755

20 Schindelin, J. *et al.* Fiji: an open-source platform for biological-image analysis. *Nat Methods* **9**, 676-682 (2012). https://doi.org:10.1038/nmeth.2019

21 Ju, Z. *et al.* Development of a robust classifier for quality control of reverse-phase protein arrays. *Bioinformatics (Oxford, England)* **31**, 912-918 (2015). https://doi.org:10.1093/bioinformatics/btu736

22 Shehwana, H. *et al.* RPPA SPACE: an R package for normalization and quantitation of Reverse-Phase Protein Array data. *Bioinformatics (Oxford, England)* **38**, 5131-5133 (2022). https://doi.org:10.1093/bioinformatics/btac665

23 Siwak, D. R., Li, J., Akbani, R., Liang, H. & Lu, Y. Analytical Platforms 3: Processing Samples via the RPPA Pipeline to Generate Large-Scale Data for Clinical Studies. *Adv Exp Med Biol* **1188**, 113-147 (2019). https://doi.org:10.1007/978-981-32-9755-5_7

24 Hoff, F. W., Lu, Y. & Kornblau, S. M. Antibody Screening. *Adv Exp Med Biol* **1188**, 149-163 (2019). https://doi.org:10.1007/978-981-32-9755-5_8

25 McGlincy, N. J. & Ingolia, N. T. Transcriptome-wide measurement of translation by ribosome profiling. *Methods* **126**, 112-129 (2017). https://doi.org:10.1016/j.ymeth.2017.05.028

26 Ingolia, N. T., Brar, G. A., Rouskin, S., McGeachy, A. M. & Weissman, J. S. The ribosome profiling strategy for monitoring translation in vivo by deep sequencing of ribosome-protected mRNA fragments. *Nature protocols* **7**, 1534 (2012). https://doi.org:10.1038/nprot.2012.086
https://www.nature.com/articles/nprot.2012.086#supplementary-information

27 Kim, D., Paggi, J. M., Park, C., Bennett, C. & Salzberg, S. L. Graph-based genome alignment and genotyping with HISAT2 and HISAT-genotype. *Nat Biotechnol* **37**, 907-915 (2019). https://doi.org:10.1038/s41587-019-0201-4

801 28 Pertea, M. *et al.* StringTie enables improved reconstruction of a transcriptome from
802 RNA-seq reads. *Nat Biotechnol* **33**, 290-295 (2015). https://doi.org:10.1038/nbt.3122
803 29 Liberzon, A. *et al.* The Molecular Signatures Database (MSigDB) hallmark gene set
804 collection. *Cell Syst* **1**, 417-425 (2015). https://doi.org:10.1016/j.cels.2015.12.004
805 30 Mootha, V. K. *et al.* PGC-1alpha-responsive genes involved in oxidative phosphorylation
806 are coordinately downregulated in human diabetes. *Nature genetics* **34**, 267-273 (2003).
807 https://doi.org:10.1038/ng1180
808 31 Korotkevich, G. *et al.* Fast gene set enrichment analysis. *bioRxiv*, 060012 (2021).
809 https://doi.org:10.1101/060012
810 32 Doench, J. G. *et al.* Optimized sgRNA design to maximize activity and minimize off-target
811 effects of CRISPR-Cas9. *Nat Biotechnol* **34**, 184-191 (2016).
812 https://doi.org:10.1038/nbt.3437
813 33 Wang, B. *et al.* Integrative analysis of pooled CRISPR genetic screens using
814 MAGeCKFlute. *Nature protocols* **14**, 756-780 (2019). https://doi.org:10.1038/s41596-
815 018-0113-7
816 34 Zheng, S. *et al.* SynergyFinder Plus: Toward Better Interpretation and Annotation of Drug
817 Combination Screening Datasets. *Genomics Proteomics Bioinformatics* **20**, 587-596
818 (2022). https://doi.org:10.1016/j.gpb.2022.01.004
819 35 Murphy, A. J. *et al.* Forty-five patient-derived xenografts capture the clinical and
820 biological heterogeneity of Wilms tumor. *Nature communications* **10**, 5806 (2019).
821 https://doi.org:10.1038/s41467-019-13646-9
822 36 Perry, R. P. & Kelley, D. E. Inhibition of RNA synthesis by actinomycin D: characteristic
823 dose-response of different RNA species. *J Cell Physiol* **76**, 127-139 (1970).
824 https://doi.org:10.1002/jcp.1040760202
825 37 Love, M. I., Huber, W. & Anders, S. Moderated estimation of fold change and dispersion
826 for RNA-seq data with DESeq2. *Genome Biol* **15**, 550 (2014).
827 https://doi.org:10.1186/s13059-014-0550-8
828 38 Cerami, E. *et al.* The cBio cancer genomics portal: an open platform for exploring
829 multidimensional cancer genomics data. *Cancer Discov* **2**, 401-404 (2012).
830 https://doi.org:10.1158/2159-8290.CD-12-0095
831 39 Gao, J. J. *et al.* Integrative Analysis of Complex Cancer Genomics and Clinical Profiles
832 Using the cBioPortal. *Sci Signal* **6** (2013). https://doi.org:ARTN pl1
833 DOI 10.1126/scisignal.2004088
834 40 Lam, Y. W., Lamond, A. I., Mann, M. & Andersen, J. S. Analysis of nucleolar protein
835 dynamics reveals the nuclear degradation of ribosomal proteins. *Curr Biol* **17**, 749-760
836 (2007). https://doi.org:10.1016/j.cub.2007.03.064
837 41 Liu, R. *et al.* Impairing the production of ribosomal RNA activates mammalian target of
838 rapamycin complex 1 signalling and downstream translation factors. *Nucleic Acids Res*
839 **42**, 5083-5096 (2014). https://doi.org:10.1093/nar/gku130
840 42 Huang, C. C. *et al.* Predicting relapse in favorable histology Wilms tumor using gene
841 expression analysis: a report from the Renal Tumor Committee of the Children's
842 Oncology Group. *Clinical cancer research : an official journal of the American Association*
843 *for Cancer Research* **15**, 1770-1778 (2009). https://doi.org:10.1158/1078-0432.CCR-08-
844 1030

845 43 Flores, L. G., 2nd *et al.* Monitoring therapy with MEK inhibitor U0126 in a novel Wilms
846 tumor model in Wt1 knockout Igf2 transgenic mice using 18F-FDG PET with dual-
847 contrast enhanced CT and MRI: early metabolic response without inhibition of tumor
848 growth. *Mol Imaging Biol* **15**, 175-185 (2013). https://doi.org:10.1007/s11307-012-0588-
849 5
850 44 Iadevaia, V., Liu, R. & Proud, C. G. mTORC1 signaling controls multiple steps in ribosome
851 biogenesis. *Semin Cell Dev Biol* **36**, 113-120 (2014).
852 https://doi.org:10.1016/j.semcdb.2014.08.004
853 45 Sung, M. K. *et al.* A conserved quality-control pathway that mediates degradation of
854 unassembled ribosomal proteins. *Elife* **5** (2016). https://doi.org:10.7554/eLife.19105
855 46 Sung, M. K., Reitsma, J. M., Sweredoski, M. J., Hess, S. & Deshaies, R. J. Ribosomal
856 proteins produced in excess are degraded by the ubiquitin-proteasome system. *Mol Biol*
857 *Cell* **27**, 2642-2652 (2016). https://doi.org:10.1091/mbc.E16-05-0290
858 47 Hanley, M. J. *et al.* Population Pharmacokinetic Analysis of Bortezomib in Pediatric
859 Leukemia Patients: Model-Based Support for Body Surface Area-Based Dosing Over the
860 2- to 16-Year Age Range. *J Clin Pharmacol* **57**, 1183-1193 (2017).
861 https://doi.org:10.1002/jcph.906
862 48 Moreau, P. *et al.* Pharmacokinetic, pharmacodynamic and covariate analysis of
863 subcutaneous versus intravenous administration of bortezomib in patients with relapsed
864 multiple myeloma. *Clin Pharmacokinet* **51**, 823-829 (2012).
865 https://doi.org:10.1007/s40262-012-0010-0
866 49 Gupta, I., Singh, K., Varshney, N. K. & Khan, S. Delineating Crosstalk Mechanisms of the
867 Ubiquitin Proteasome System That Regulate Apoptosis. *Front Cell Dev Biol* **6**, 11 (2018).
868 https://doi.org:10.3389/fcell.2018.00011
869 50 Ling, Y. H. *et al.* Mechanisms of proteasome inhibitor PS-341-induced G(2)-M-phase
870 arrest and apoptosis in human non-small cell lung cancer cell lines. *Clinical cancer*
871 *research : an official journal of the American Association for Cancer Research* **9**, 1145-
872 1154 (2003).
873 51 Nawrocki, S. T. *et al.* Effects of the proteasome inhibitor PS-341 on apoptosis and
874 angiogenesis in orthotopic human pancreatic tumor xenografts. *Mol Cancer Ther* **1**,
875 1243-1253 (2002).
876 52 Selimovic, D. *et al.* Bortezomib/proteasome inhibitor triggers both apoptosis and
877 autophagy-dependent pathways in melanoma cells. *Cell Signal* **25**, 308-318 (2013).
878 https://doi.org:10.1016/j.cellsig.2012.10.004
879 53 Bao, X. *et al.* Bortezomib induces apoptosis and suppresses cell growth and metastasis
880 by inactivation of Stat3 signaling in chondrosarcoma. *Int J Oncol* **50**, 477-486 (2017).
881 https://doi.org:10.3892/ijo.2016.3806
882 54 Lou, Z. *et al.* Bortezomib induces apoptosis and autophagy in osteosarcoma cells through
883 mitogen-activated protein kinase pathway in vitro. *J Int Med Res* **41**, 1505-1519 (2013).
884 https://doi.org:10.1177/0300060513490618
885 55 Hofmann, J. F. & Beach, D. cdt1 is an essential target of the Cdc10/Sct1 transcription
886 factor: requirement for DNA replication and inhibition of mitosis. *EMBO J* **13**, 425-434
887 (1994). https://doi.org:10.1002/j.1460-2075.1994.tb06277.x

888 56 Fagundes, R. & Teixeira, L. K. Cyclin E/CDK2: DNA Replication, Replication Stress and
889 Genomic Instability. *Front Cell Dev Biol* **9**, 774845 (2021).
890 https://doi.org:10.3389/fcell.2021.774845
891 57 Caldon, C. E. & Musgrove, E. A. Distinct and redundant functions of cyclin E1 and cyclin
892 E2 in development and cancer. *Cell Div* **5**, 2 (2010). https://doi.org:10.1186/1747-1028-
893 5-2
894 58 Pozo, P. N. & Cook, J. G. Regulation and Function of Cdt1; A Key Factor in Cell
895 Proliferation and Genome Stability. *Genes (Basel)* **8** (2016).
896 https://doi.org:10.3390/genes8010002
897 59 Martinez-Alonso, D. & Malumbres, M. Mammalian cell cycle cyclins. *Semin Cell Dev Biol*
898 **107**, 28-35 (2020). https://doi.org:10.1016/j.semcdb.2020.03.009
899 60 Kaufmann, S. H., Desnoyers, S., Ottaviano, Y., Davidson, N. E. & Poirier, G. G. Specific
900 proteolytic cleavage of poly(ADP-ribose) polymerase: an early marker of chemotherapy-
901 induced apoptosis. *Cancer Res* **53**, 3976-3985 (1993).
902 61 Kaufmann, S. H. Induction of endonucleolytic DNA cleavage in human acute
903 myelogenous leukemia cells by etoposide, camptothecin, and other cytotoxic anticancer
904 drugs: a cautionary note. *Cancer Res* **49**, 5870-5878 (1989).
905 62 Boulares, A. H. *et al.* Role of poly(ADP-ribose) polymerase (PARP) cleavage in apoptosis.
906 Caspase 3-resistant PARP mutant increases rates of apoptosis in transfected cells. *J Biol*
907 *Chem* **274**, 22932-22940 (1999). https://doi.org:10.1074/jbc.274.33.22932
908 63 Rager, J. E. in *Systems Biology in Toxicology and Environmental Health* 187-205 (2015).
909 64 Stewart, E. *et al.* Orthotopic patient-derived xenografts of paediatric solid tumours.
910 *Nature* **549**, 96-100 (2017). https://doi.org:10.1038/nature23647
911 65 Walz, A. L. *et al.* Recurrent DGCR8, DROSHA, and SIX homeodomain mutations in
912 favorable histology Wilms tumors. *Cancer cell* **27**, 286-297 (2015).
913 https://doi.org:10.1016/j.ccell.2015.01.003
914 66 Wegert, J. *et al.* Mutations in the SIX1/2 pathway and the DROSHA/DGCR8 miRNA
915 microprocessor complex underlie high-risk blastemal type Wilms tumors. *Cancer cell* **27**,
916 298-311 (2015). https://doi.org:10.1016/j.ccell.2015.01.002
917 67 Torrezan, G. T. *et al.* Recurrent somatic mutation in DROSHA induces microRNA profile
918 changes in Wilms tumour. *Nature communications* **5**, 4039 (2014).
919 https://doi.org:10.1038/ncomms5039
920 68 Rakheja, D. *et al.* Somatic mutations in DROSHA and DICER1 impair microRNA biogenesis
921 through distinct mechanisms in Wilms tumours. *Nature communications* **2**, 4802 (2014).
922 https://doi.org:10.1038/ncomms5802
923 69 Tiburcio, P. D. B. *et al.* DROSHA regulates mesenchymal gene expression in Wilms tumor.
924 *Mol Cancer Res* (2024). https://doi.org:10.1158/1541-7786.MCR-23-0930
925 70 Matthews, H. K., Bertoli, C. & de Bruin, R. A. M. Cell cycle control in cancer. *Nat Rev Mol*
926 *Cell Biol* **23**, 74-88 (2022). https://doi.org:10.1038/s41580-021-00404-3
927 71 Zou, T. & Lin, Z. The Involvement of Ubiquitination Machinery in Cell Cycle Regulation
928 and Cancer Progression. *Int J Mol Sci* **22** (2021). https://doi.org:10.3390/ijms22115754
929 72 Alber, A. B. & Suter, D. M. Dynamics of protein synthesis and degradation through the
930 cell cycle. *Cell Cycle* **18**, 784-794 (2019).
931 https://doi.org:10.1080/15384101.2019.1598725

932 73 Mayer, C., Zhao, J., Yuan, X. & Grummt, I. mTOR-dependent activation of the
933 transcription factor TIF-IA links rRNA synthesis to nutrient availability. *Genes Dev* **18**,
934 423-434 (2004). https://doi.org:10.1101/gad.285504
935 74 Mayer, C. & Grummt, I. Ribosome biogenesis and cell growth: mTOR coordinates
936 transcription by all three classes of nuclear RNA polymerases. *Oncogene* **25**, 6384-6391
937 (2006). https://doi.org:10.1038/sj.onc.1209883
938 75 Ni, C. & Buszczak, M. The homeostatic regulation of ribosome biogenesis. *Semin Cell Dev*
939 *Biol* **136**, 13-26 (2023). https://doi.org:10.1016/j.semcdb.2022.03.043
940 76 Hua, H. *et al.* Targeting mTOR for cancer therapy. *J Hematol Oncol* **12**, 71 (2019).
941 https://doi.org:10.1186/s13045-019-0754-1
942 77 Saxton, R. A. & Sabatini, D. M. mTOR Signaling in Growth, Metabolism, and Disease. *Cell*
943 **168**, 960-976 (2017). https://doi.org:10.1016/j.cell.2017.02.004
944 78 Zou, Z., Tao, T., Li, H. & Zhu, X. mTOR signaling pathway and mTOR inhibitors in cancer:
945 progress and challenges. *Cell Biosci* **10**, 31 (2020). https://doi.org:10.1186/s13578-020-
946 00396-1
947 79 Park, S. H., Choi, W. H. & Lee, M. J. Effects of mTORC1 inhibition on proteasome activity
948 and levels. *BMB Rep* **55**, 161-165 (2022).
949 https://doi.org:10.5483/BMBRep.2022.55.4.032
950 80 Tye, B. W. *et al.* Proteotoxicity from aberrant ribosome biogenesis compromises cell
951 fitness. *Elife* **8** (2019). https://doi.org:10.7554/eLife.43002
952 81 Zhang, Y. & Manning, B. D. mTORC1 signaling activates NRF1 to increase cellular
953 proteasome levels. *Cell Cycle* **14**, 2011-2017 (2015).
954 https://doi.org:10.1080/15384101.2015.1044188
955 82 Zhang, Y. *et al.* Coordinated regulation of protein synthesis and degradation by mTORC1.
956 *Nature* **513**, 440-443 (2014). https://doi.org:10.1038/nature13492
957 83 Zhao, J., Zhai, B., Gygi, S. P. & Goldberg, A. L. mTOR inhibition activates overall protein
958 degradation by the ubiquitin proteasome system as well as by autophagy. *Proc Natl Acad*
959 *Sci U S A* **112**, 15790-15797 (2015). https://doi.org:10.1073/pnas.1521919112
960 84 Kaiser, M. S. *et al.* Dual roles of mTORC1-dependent activation of the ubiquitin-
961 proteasome system in muscle proteostasis. *Commun Biol* **5**, 1141 (2022).
962 https://doi.org:10.1038/s42003-022-04097-y
963 85 Chen, D., Frezza, M., Schmitt, S., Kanwar, J. & Dou, Q. P. Bortezomib as the First
964 Proteasome Inhibitor Anticancer Drug: Current Status and Future Perspectives. *Current*
965 *Cancer Drug Targets* **11**, 239-253 (2011). https://doi.org:Doi
966 10.2174/156800911794519752
967 86 Leonardo-Sousa, C. *et al.* Revisiting Proteasome Inhibitors: Molecular Underpinnings of
968 Their Development, Mechanisms of Resistance and Strategies to Overcome Anti-Cancer
969 Drug Resistance. *Molecules* **27** (2022). https://doi.org:10.3390/molecules27072201
970 87 Lu, S. & Wang, J. The resistance mechanisms of proteasome inhibitor bortezomib.
971 *Biomark Res* **1**, 13 (2013). https://doi.org:10.1186/2050-7771-1-13
972 88 August, K. J., Guest, E. M., Lewing, K., Hays, J. A. & Gamis, A. S. Treatment of children
973 with relapsed and refractory acute lymphoblastic leukemia with mitoxantrone,
974 vincristine, pegaspargase, dexamethasone, and bortezomib. *Pediatr Blood Cancer* **67**,
975 e28062 (2020). https://doi.org:10.1002/pbc.28062

89 Teachey, D. T. *et al.* Children's Oncology Group Trial AALL1231: A Phase III Clinical Trial Testing Bortezomib in Newly Diagnosed T-Cell Acute Lymphoblastic Leukemia and Lymphoma. *Journal of clinical oncology : official journal of the American Society of Clinical Oncology* **40**, 2106-2118 (2022). https://doi.org:10.1200/JCO.21.02678

90 Styczynski, J., Olszewska-Slonina, D., Kolodziej, B., Napieraj, M. & Wysocki, M. Activity of bortezomib in glioblastoma. *Anticancer Res* **26**, 4499-4503 (2006).

91 Chang, D., Chen, F., Zhang, F., McKay, B. C. & Ljungman, M. Dose-dependent effects of DNA-damaging agents on p53-mediated cell cycle arrest. *Cell Growth Differ* **10**, 155-162 (1999).

92 Chen, C. S. *et al.* AKT mediates actinomycin D-induced p53 expression. *Oncotarget* **5**, 693-703 (2014). https://doi.org:10.18632/oncotarget.1328

93 Yang, V. W. in *Physiology of the Gastrointestinal Tract* 197-219 (2018).

94 Santo, L., Siu, K. T. & Raje, N. Targeting Cyclin-Dependent Kinases and Cell Cycle Progression in Human Cancers. *Semin Oncol* **42**, 788-800 (2015). https://doi.org:10.1053/j.seminoncol.2015.09.024

95 Chu, C., Geng, Y., Zhou, Y. & Sicinski, P. Cyclin E in normal physiology and disease states. *Trends Cell Biol* **31**, 732-746 (2021). https://doi.org:10.1016/j.tcb.2021.05.001

96 Voutsadakis, I. A. Proteasome expression and activity in cancer and cancer stem cells. *Tumour Biol* **39**, 1010428317692248 (2017). https://doi.org:10.1177/1010428317692248

97 Lagadec, C. *et al.* Tumor cells with low proteasome subunit expression predict overall survival in head and neck cancer patients. *BMC Cancer* **14**, 152 (2014). https://doi.org:10.1186/1471-2407-14-152

98 Byers, H. A. *et al.* Evaluation of the NRF1-proteasome axis as a therapeutic target in breast cancer. *Sci Rep* **13**, 15843 (2023). https://doi.org:10.1038/s41598-023-43121-x

99 He, W. *et al.* PSMB2 plays an oncogenic role in glioma and correlates to the immune microenvironment. *Sci Rep* **14**, 5861 (2024). https://doi.org:10.1038/s41598-024-56493-5

100 Liu, J., Mi, J., Liu, S., Chen, H. & Jiang, L. PSMB5 overexpression is correlated with tumor proliferation and poor prognosis in hepatocellular carcinoma. *FEBS Open Bio* **12**, 2025-2041 (2022). https://doi.org:10.1002/2211-5463.13479

101 Walerych, D. *et al.* Proteasome machinery is instrumental in a common gain-of-function program of the p53 missense mutants in cancer. *Nat Cell Biol* **18**, 897-909 (2016). https://doi.org:10.1038/ncb3380

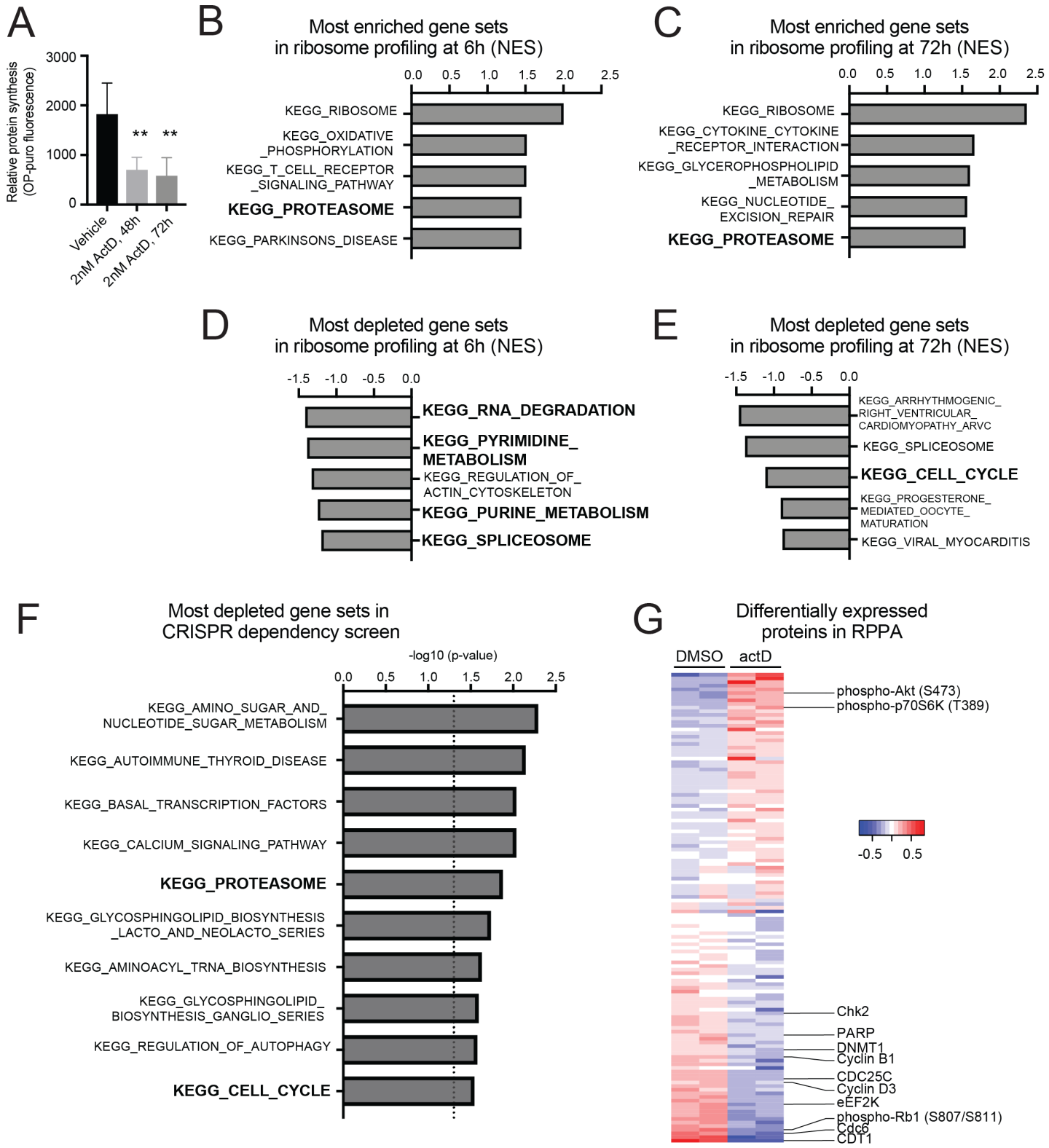

Figure 1. ActD disrupts protein homeostasis in anaplastic Wilms tumor cells

(A) Quantification of protein synthesis assay (OPP incorporation) in WiT49 cells treated with 48 and 72 hours of 2nM actD or vehicle DMSO. **(B,C)** Most enriched KEGG gene sets in ribosome profiling of actD- vs. DMSO-treated WiT49 after 6 hours **(B)** or 72 hours **(C)**. **(D,E)** Most depleted KEGG gene sets in ribosome profiling of actD- vs. DMSO-treated WiT49 after 6 hours **(D)** or 72 hours **(E)**. **(F)** GSEA of genome-wide CRISPR knockout library screen reveals top 10 most significant KEGG canonical pathways that sensitize WiT49 to actD pathways, ranked by p-value. Highlighted are the KEGG_PROTEASOME and KEGG_CELL_CYCLE, where the dotted line represents p-value at 0.05. **(G)** Heatmap displaying results from RPPA of actD- versus DMSO-treated WiT49. Normalized, log2-transformed, median-centered values from validated antibodies with standard deviation over 0.1 are shown here.

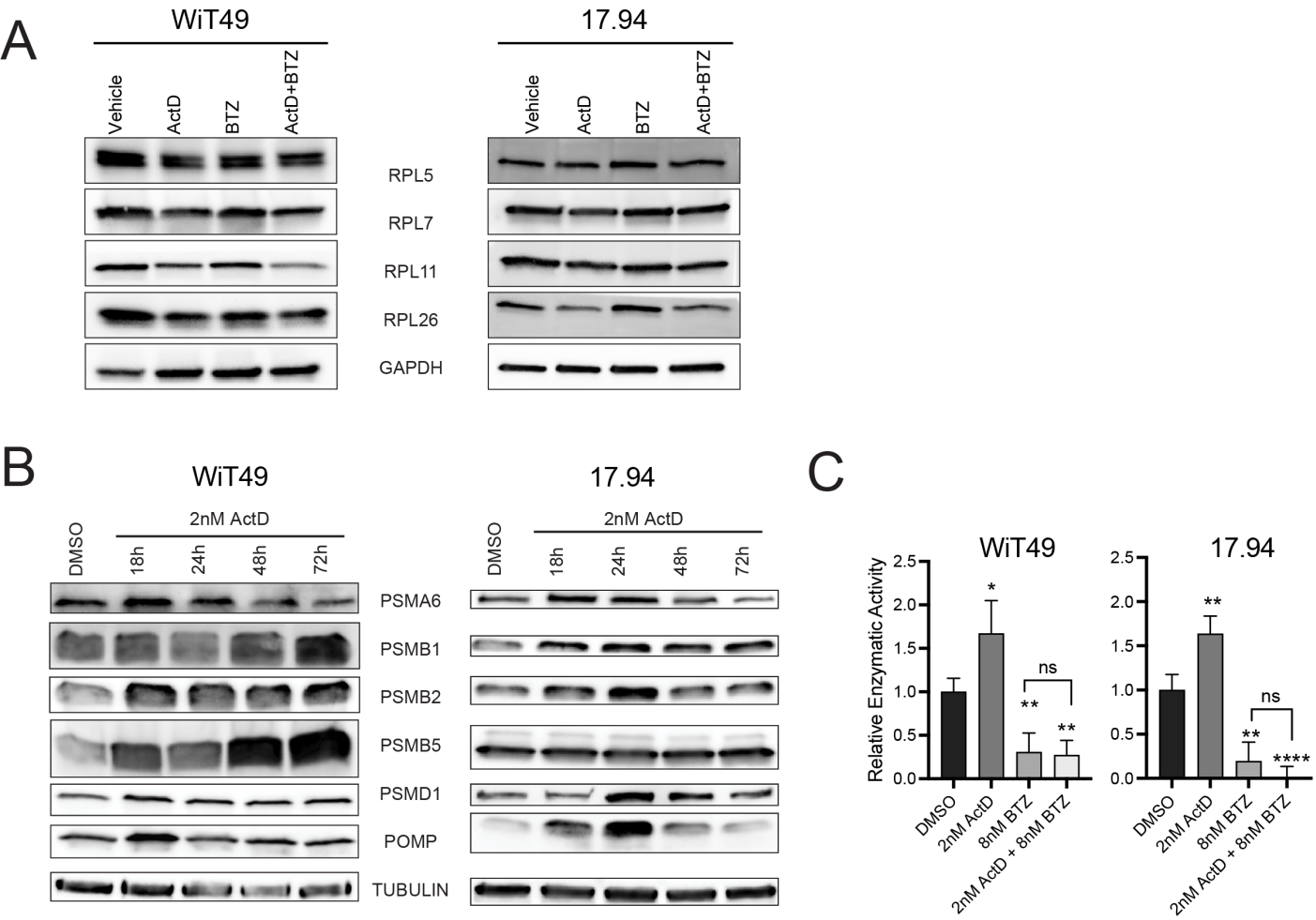

Figure 2. ActD promotes proteasome level and activity in anaplastic Wilms tumor cells
(A) Western blots for ribosomal protein subunits RPL5, RPL7, RPL11, and RPL26 in WiT49 and 17.94 following 48-hour treatment of DMSO, 2nM actD, 8nM BTZ, or 2nM ActD + 8nM BTZ. **(B)** Protein levels of proteasome subunits PSMA6 (α1), PSMB1 (β6), PSMB2 (β4), PSMB5 (β5), and PSMD1 (P112), and POMP in WiT49 and 17.94 following 18-, 24-, 48-, and 72-hour 2nM actD treatment versus vehicle (DMSO). **(C)** Quantification of relative proteasome-specific chymotrypsin-like activity in WiT49 and 17.94 cells following 24 hours of DMSO versus 2nM actD, 8nM BTZ, or 2nM actD + 8nM BTZ treatments (Student's t-test p-value versus vehicle: *<0.05, ** <0.01, ****<0.0001).

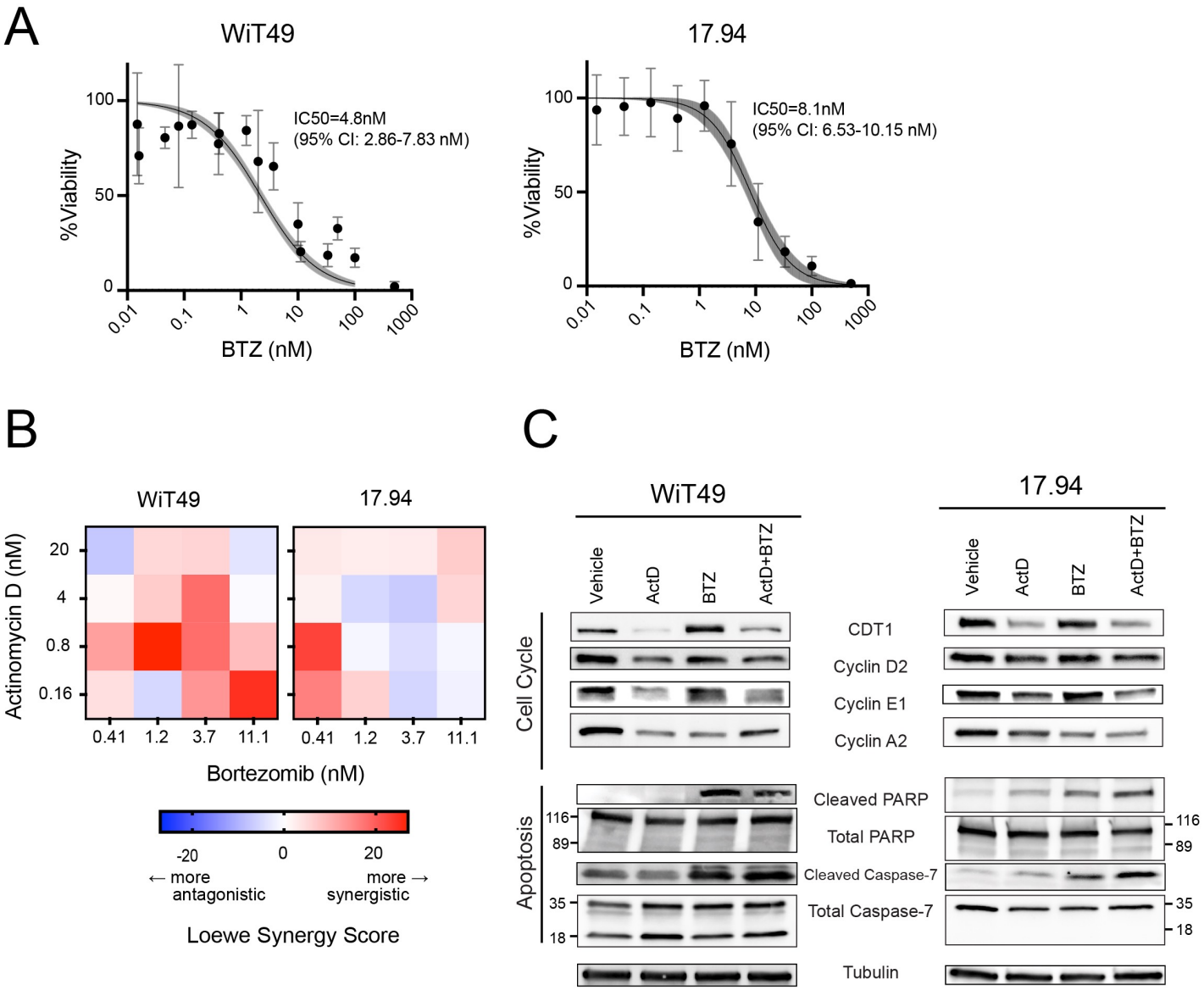

Figure 3. BTZ sensitizes anaplastic Wilms tumor cell lines to actD in vitro
(A) BTZ kill curves for WiT49 and 17.94 with IC50 values indicated (four-point regression line with shaded region representing 95% confidence interval). **(B)** Heat maps of Loewe synergy scores for combinations of actD and BTZ in WiT49 and 17.94 cells. **(C)** Effect of 48-hour treatment WiT49 and 17.94 cells with DMSO, actD, BTZ, and combination actD + BTZ on cell cycle and apoptosis markers by Western blot.

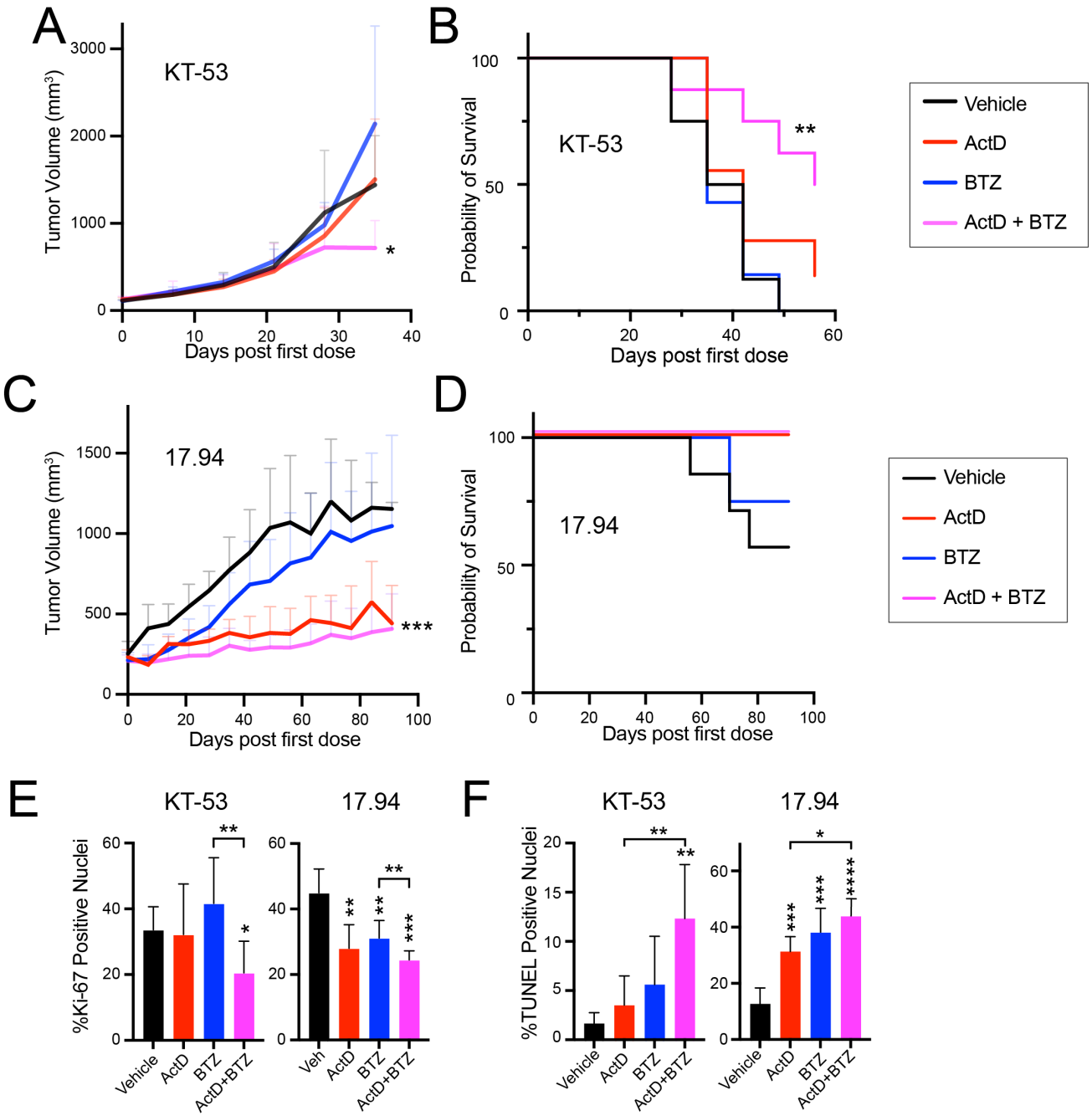

Figure 4. BTZ sensitizes subcutaneous anaplastic Wilms tumor xenografts to actD

(A) Subcutaneous tumor volumes of NSG mice bearing KT-53 xenografts treated with vehicle, actD, BTZ, and combination actD + BTZ (Student's t-test of endpoint volumes of combination versus vehicle or actD only: * <0.05). **(B)** Kaplan-Meier survival curves for KT-53 tumor-bearing mice treated with vehicle, actD only, BTZ only, and combination (log-rank test versus vehicle ** <0.01).**(C)** Subcutaneous tumor volumes of NSG mice bearing 17.94 xenografts treated with vehicle, actD only, BTZ only, and combination (Student's t-test of endpoint volumes of combination versus vehicle: ***<0.001). **(D)** Kaplan-Meier survival curves for 17.94 tumor-bearing mice treated with vehicle, actD only, BTZ only, and combination. **(E,F)** Quantification of Ki-67 positive nuclei (E) and TUNEL positive nuclei (F) in in KT-53 and 17.94 subcutaneous tumors treated with vehicle, actD only, BTZ only, or combination actD + BTZ (Student's t-test p-value versus vehicle unless otherwise indicated: * <0.05, **<0.01, ***<0.001, ****<0.0001).

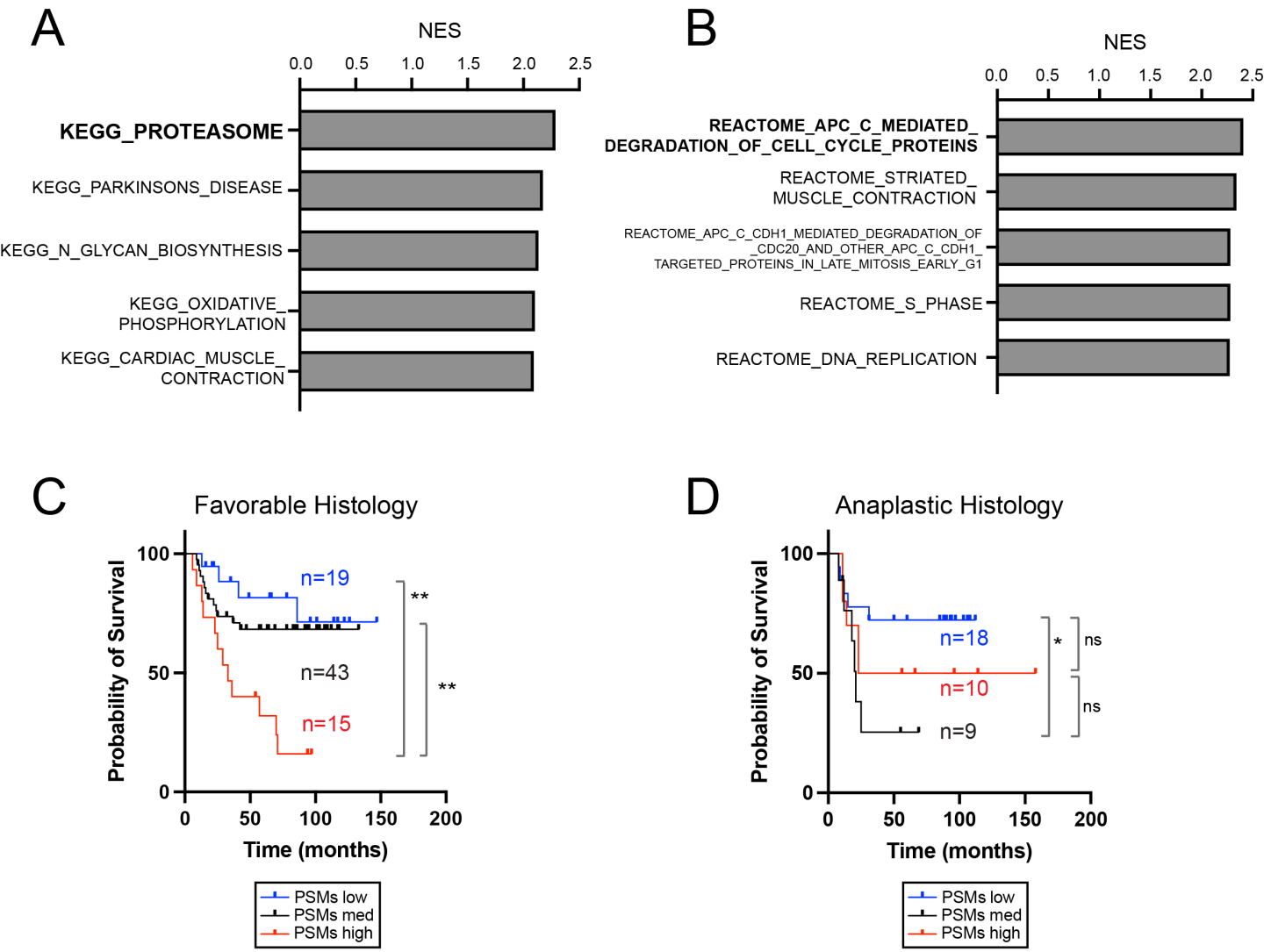

Figure 5. RNA expression of proteasome genes in TARGET favorable and anaplastic histology Wilms tumors

(A) Top KEGG pathways enriched in RNA-seq of DAWT versus FHWT. **(B)** Top reactome pathways enriched in RNA-seq of DAWT versus FHWT. **(C,D)** Overall survival of tumors stratified according to expression of proteasome enzymatic subunit genes PSMB1, PSMB2, PSMB5 among patients with favorable histology tumors **(C)** or anaplastic histology **(D)**. (Log Rank test p-value: *<0.05, ** 0.01)

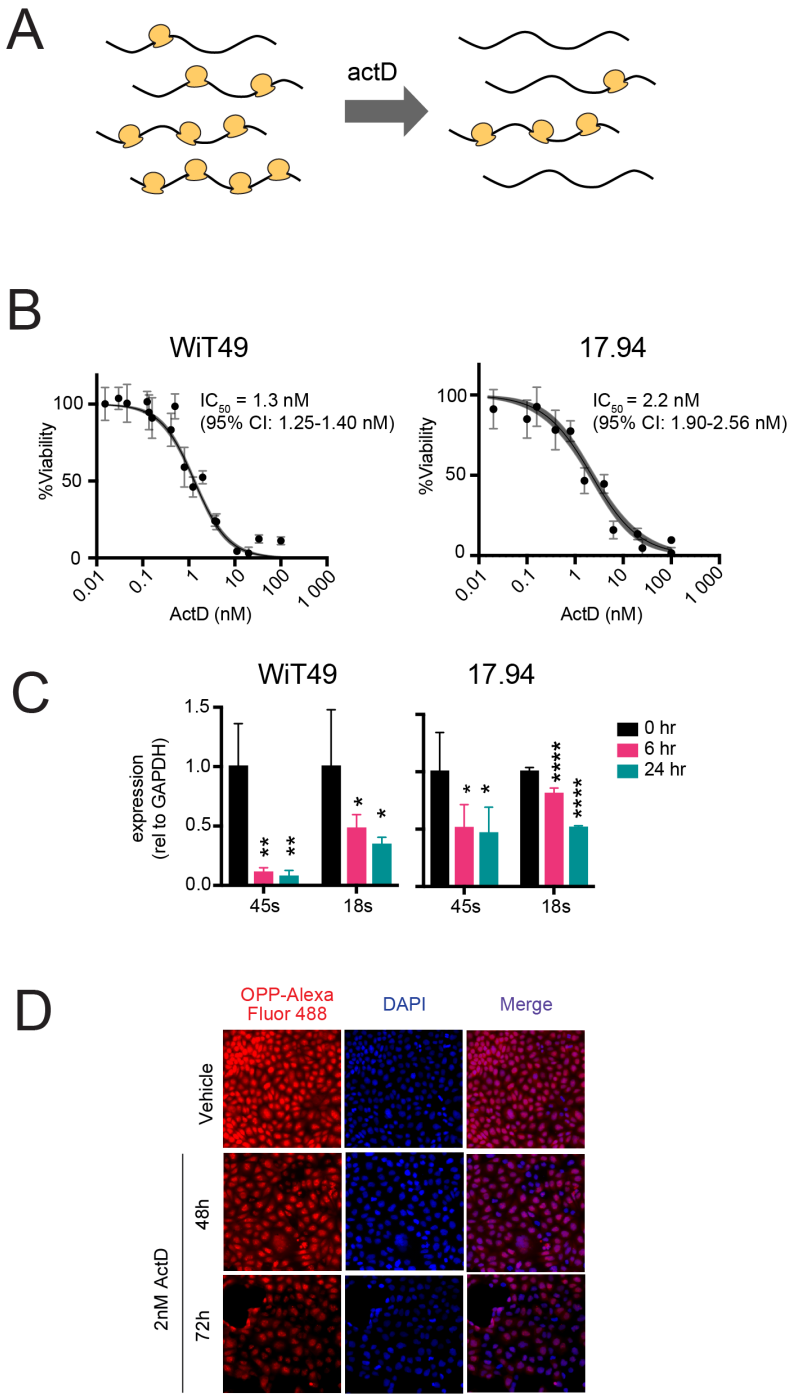

Supplementary Figure S1. ActD alters global translation in WiT49 anaplastic Wilms tumor cells
(A) Diagram of the effect of actD on Wilms tumor cells at the translational level. ActD depletes fully-formed ribosomes and reduces translational capacity. The reduced ribosomes are distributed unevenly, resulting in an altered translational landscape. Identification of the ribosomal footprints by ribosome profiling provides a snapshot of transcripts actively undergoing translation. **(B)** ActD kill curves for anaplastic Wilms Tumor cell lines WiT49 and 17.94 with IC50 values indicated (four-point regression line with shaded region representing 95% confidence interval). **(C)** Levels of 45s pre-rRNA and 18s mature rRNA in anaplastic Wilms tumor cell lines WiT49 and 17.94, quantified by qPCR following actD treatment for 6 and 24 hours. **(D)** Micrographs of protein synthesis assay. Red fluorescence measures OPP incorporation relative to total area of WiT49 cells treated with 48 and 72 hours of 2nM actD or vehicle DMSO.

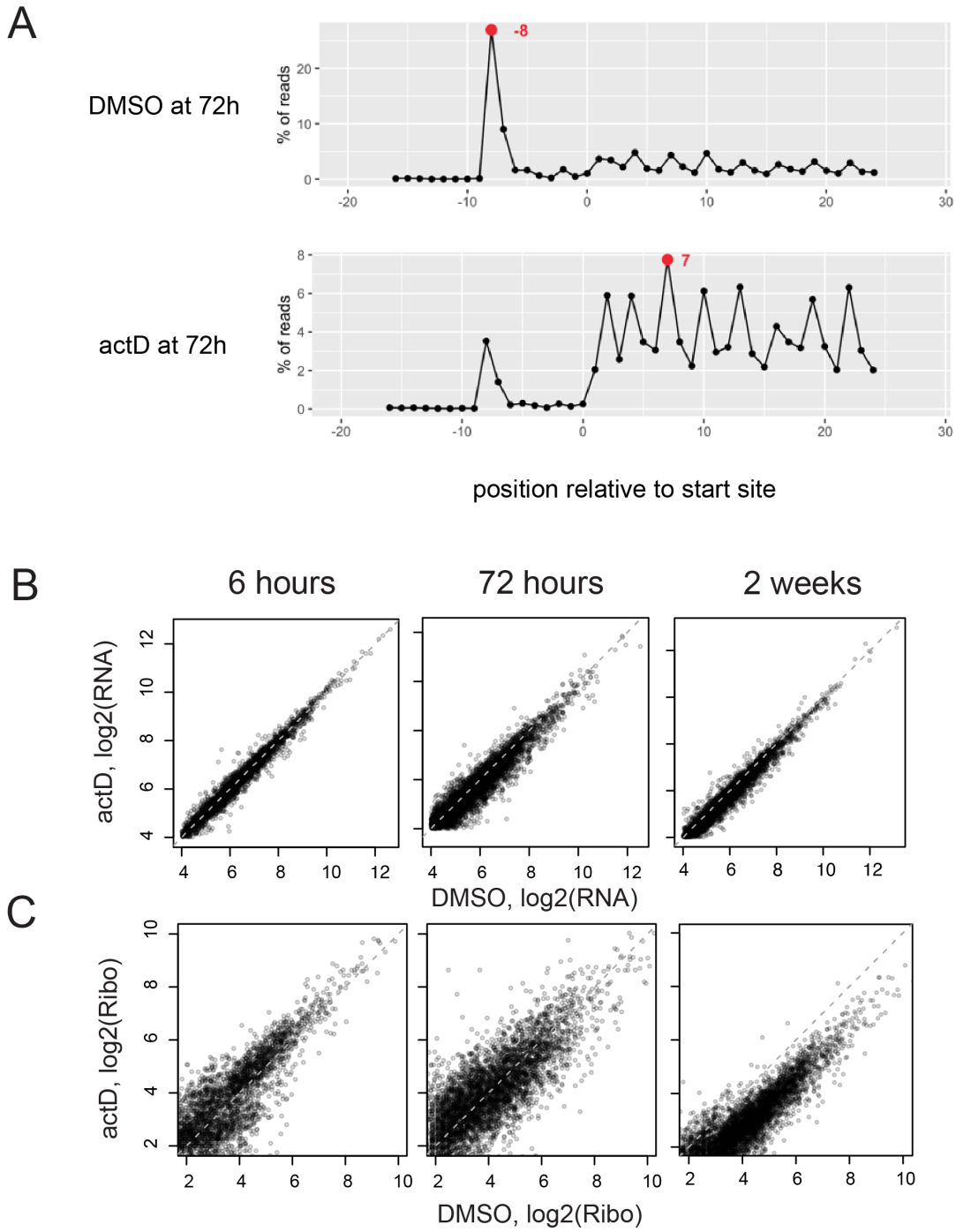

Supplementary Figure S2. Ribosome profiling metrics in actD-treated WiT49.
(A) Position of left edge of ribosome footprints relative to translation initiation site (0), on the top 30% most abundant transcripts, in DMSO and actD samples at 72 hours. Peak position highlighted in red. **(B,C)** Log2-transformed counts aligning to each gene, by RNA-seq **(B)** and translation efficiency by ribosome profiling **(C)** after 6-hour, 72-hour, and 2-week treatments of WiT49 with actD (y-axes) versus DMSO (x-axes).

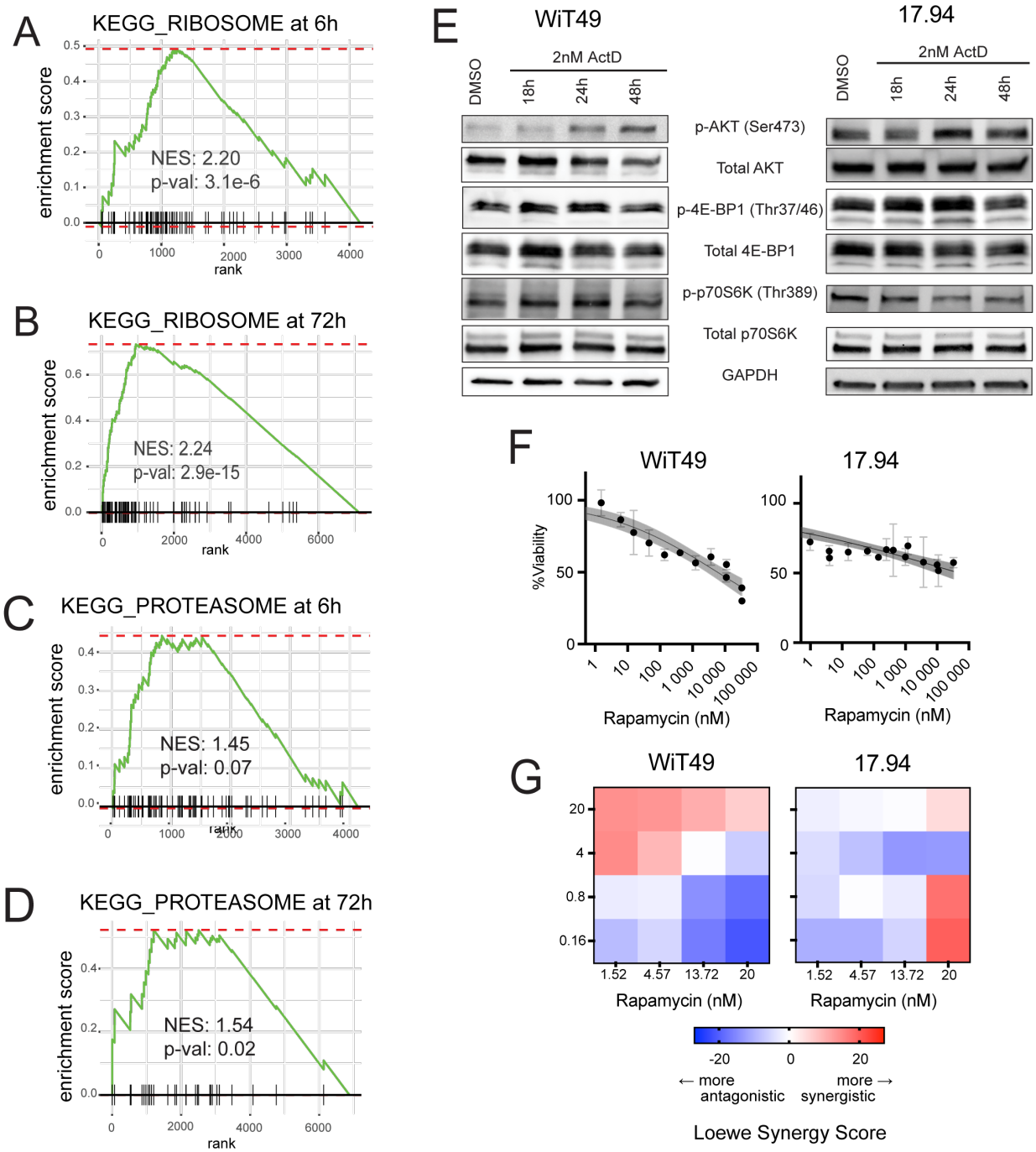

Supplementary Figure S3. ActD induces translation of ribosome and proteasome subunits and upregulates Akt/mTOR signaling.

(A,B) KEGG_ RIBOSOME pathway enrichment plots after 6 hours **(A)** and 72 hours **(B)** of exposure to actD versus DMSO. (NES, Normalized Enrichment Score). **(C,D)** KEGG_ PROTEASOME pathway enrichment plots after 6 hours **(C)** and 72 hours **(D)** of exposure to actD versus DMSO. (NES, Normalized Enrichment Score). **(E)** Changes in phosphorylation of Akt/mTOR signaling components visualized by western blot in WiT49 and 17.94 following 2nM actD treatment versus vehicle (DMSO). **(F)** Rapamycin kill curves for anaplastic Wilms Tumor cell lines WiT49 and 17.94 (four-point regression line with shaded region representing 95% confidence interval). **(G)** Heat maps of Loewe synergy scores for combinations of actD and rapamycin in WiT49 and 17.94 cells.

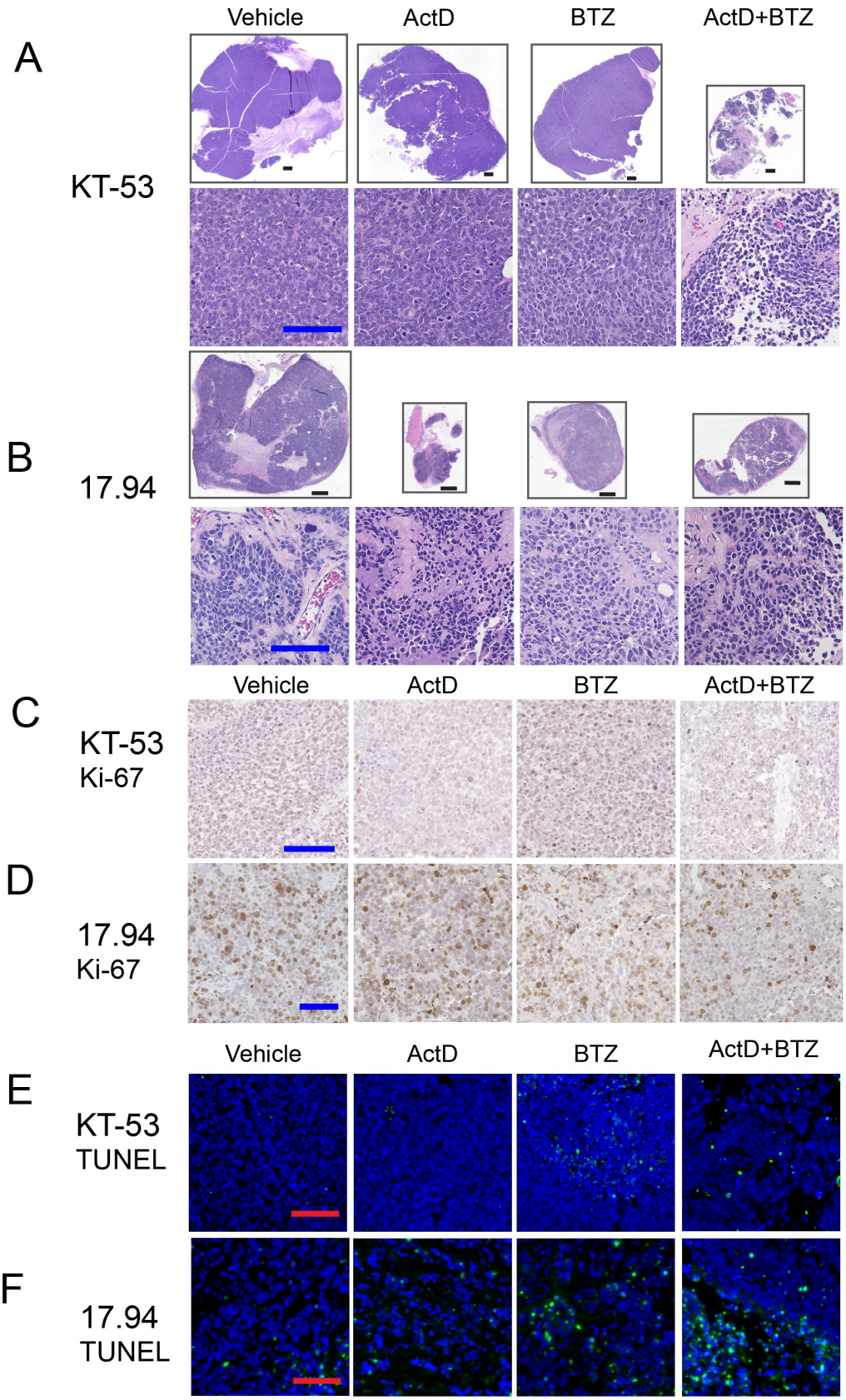

Supplementary Figure S4. Bortezomib enhances cytotoxicity of actinomycin D in anaplastic Wilms tumor xenografts.

(A,B) Low-power and high-power H&E images of **(A)** KT-53 and **(B)** 17.94 subcutaneous tumors (Black bar = 1.0 mm; Blue Bar =100 μm) **(C, D)** High-power photomicrographs of Ki-67 immunohistochemistry of KT-53 (Bar =100 μm) **(C)** and 17.94 **(D)**. **(E, F)** High-power photomicrographs of TUNEL stain of KT-53 (Bar =100 μm) **(E)** and 17.94 **(F)**.

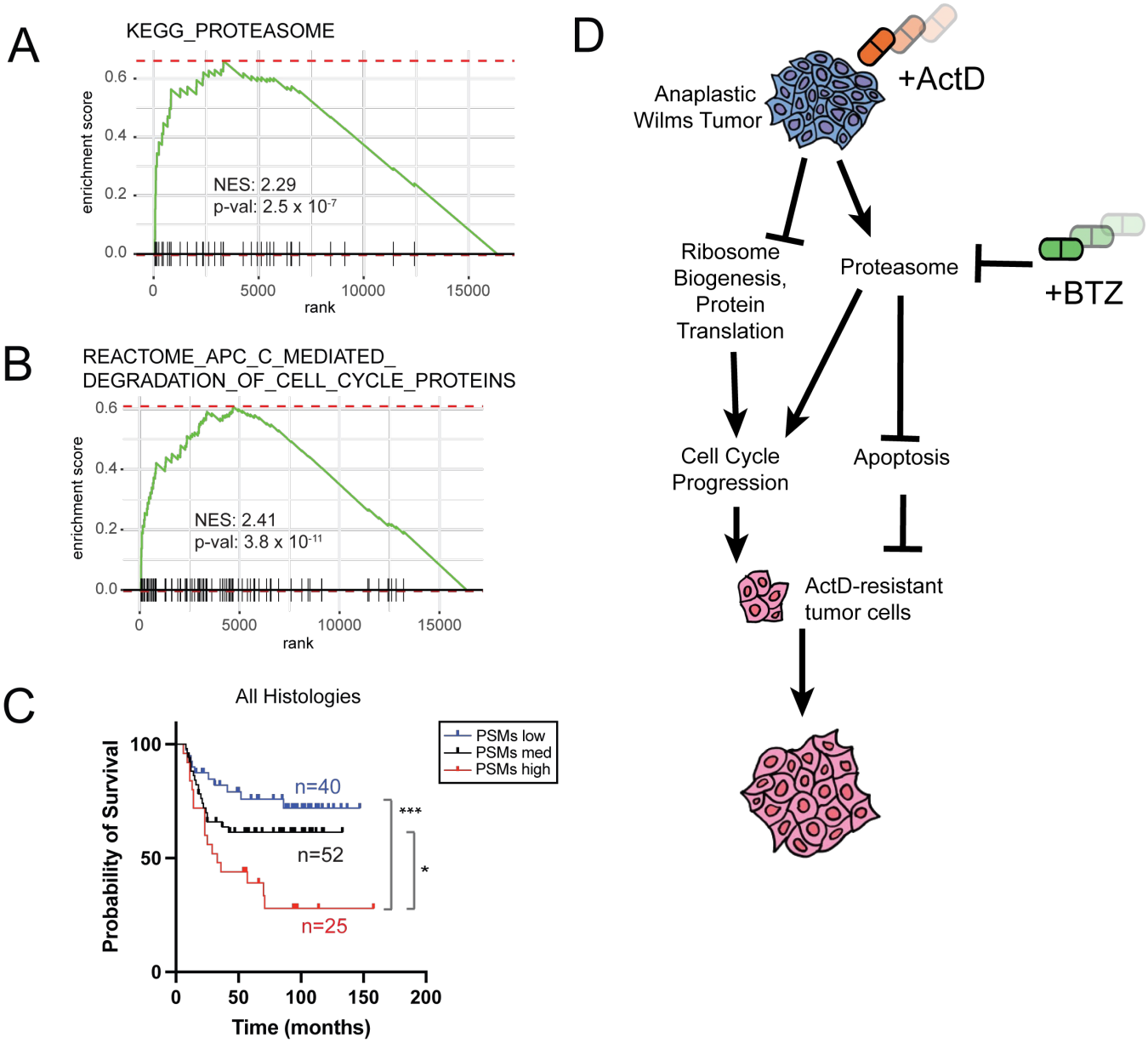

Supplementary Figure S5. Enrichment for proteasome gene sets in anaplastic Wilms tumor.
(A,B) GSEA plot showing enrichment for KEGG_PROTEASOME **(A)** and REACTOME_APC_C_MEDIATED_DEGRADATION_OF_CELL_CYCLE_PROTEINS **(B)** in anaplastic Wilms tumor vs. favorable-histology Wilms tumors in TARGET dataset.
(C) Overall survival of Wilms tumors, regardless of histology, stratified according to expression of proteasome enzymatic subunit genes PSMB1, PSMB2, PSMB5 among patients (Log rank test p-value: *<0.05, *** 0.001).
(D) Model for effect of actinomycin D on protein homeostasis in Wilms tumor cells.